

Reduced order modeling for nonlinear structural analysis using Gaussian process regression

Mengwu Guo*, Jan S. Hesthaven

*Chair of Computational Mathematics and Simulation Science,
École Polytechnique Fédérale de Lausanne, 1015 Lausanne, Switzerland*

Abstract

A non-intrusive reduced basis (RB) method is proposed for parametrized nonlinear structural analysis undergoing large deformations and with elasto-plastic constitutive relations. In this method, a reduced basis is constructed from a set of full-order snapshots by the proper orthogonal decomposition (POD), and the Gaussian process regression (GPR) is used to approximate the projection coefficients. The GPR is carried out in the offline stage with active data selection, and the outputs for new parameter values can be obtained rapidly as probabilistic distributions during the online stage. Due to the complete decoupling of the offline and online stages, the proposed non-intrusive RB method provides a powerful tool to efficiently solve parametrized nonlinear problems with various engineering applications requiring multi-query or real-time evaluations. With both geometric and material nonlinearities taken into account, numerical results are presented for typical 1D and 3D examples, illustrating the accuracy and efficiency of the proposed method.

Keywords: Reduced basis method, nonlinear structural analysis, proper orthogonal decomposition, Gaussian process regression, machine learning

1. Introduction

Models expressed as *parametrized nonlinear partial differential equations* are widely used in structural engineering [20, 38]. In such models, parameters are defined to characterize material properties, loads, geometric features, boundary conditions and so on. Especially in the context of *multi-query* or *real-time* structural analysis, such as structural optimization [14], reliability analysis [29], real-time updating [24] and parameter estimation [10], it is required to solve the system for many parameter values.

The rapid development of computer-aided engineering (CAE) and simulation science during the past several decades has enabled high-fidelity simulations for complex engineering structures, for which finite element methods (FEMs) [48, 49] are the most popular tools and have been widely studied and used. In spite of the increasing computational power, high-fidelity simulations are still too expensive to allow multi-query or real-time problems, as a large amount of degrees of freedom (DOFs) are required to accurately solve a problem, implying great demands on both CPU time and memory. Due to some intrinsic similarities among the solutions at different parameter values, on the other side, repeatable high-fidelity calculations for varying parameters are potentially wasting substantial computational resource. To address this issue, reduced order modeling (ROM) has been extensively developed for decades, aiming at reducing the computational cost with a controlled loss of accuracy. The key idea of ROM is to replace the full-order system with a carefully constructed reduced-order model with much smaller dimension, to reduce memory needs and CPU time.

The *reduced basis (RB) method* [20, 37, 38, 41] is a powerful and widely used technique for ROM, carried out in an offline-online framework. In the *offline* stage, an RB space, with a significantly smaller dimension

*Corresponding author.

Email addresses: mengwu.guo@epfl.ch (Mengwu Guo), Jan.Hesthaven@epfl.ch (Jan S. Hesthaven)

20 than the full-order problem, is spanned by a set of RB functions carefully extracted from a set of high-fidelity
21 snapshots obtained at specific parameter locations. The two major approaches for such extraction are the
22 *Greedy algorithm* [13, 37] and the *proper orthogonal decomposition* (POD) [26, 38], of which the former
23 selects a subset of snapshots as basis functions according to some optimality criterion, while the latter
24 employs a singular value decomposition (SVD) to the collection of snapshots to recover the RB functions.
25 Once the RB space is constructed, the approximated solution for a desired new parameter value is sought
26 *online* as a linear combination of the RB functions. A Galerkin projection is often employed to determine
27 the combination coefficients, and referred to as the Galerkin-projection-based approach for the online stage.

28 The success of the RB method in decreasing computational cost relies on the decoupling of the offline
29 and online stages, ensuring that the online computation is independent of the dimension of the full-order
30 model. For a general nonlinear structural problem with non-affine dependence on parameters, however, such
31 a full decoupling is often not possible. The assembly of the reduced problem is directly embodied online,
32 and both the configuration updating and the nonlinear iteration require the full-order model, which leads
33 to a reduced efficiency. The empirical interpolation method (EIM) [2] and its discrete variants [12, 32] have
34 been proposed to recover an affine expansion of the differential operator in a non-affine case. However, such
35 schemes are problem-dependent and of an *intrusive* nature, and is often not practical for complex nonlinear
36 problems.

37 The research on the reduced order modeling for structural analysis began in the 1980's [36]. Because
38 of the complexity in the constitutive relations of solid materials and the nonlinearity due to the large
39 deformation, the construction of reduced models is usually challenging for structural problems. However,
40 various techniques for reducing different structural models have been proposed, such as the model order
41 reduction for nonlinear structural dynamics [1, 25], the reduced basis method for many-parameter structural
42 problems [30], the reduced basis method for finite deformation [47], and some hyper-reduction techniques
43 for structural analysis [9, 11, 39], etc. Basically all these existing methods are intrusive, and sometimes
44 inconvenient for practical applications in engineering.

45 In this paper, a non-intrusive RB method is proposed for nonlinear structural analysis. After extracting
46 the RB functions from a set of snapshots by POD, a regression-based approach [21] is used to establish a
47 mapping from parameter values to projection coefficients onto the RB space. A complete decoupling of offline
48 and online stages is ensured by the regression-based approach, as the online solutions only require direct
49 outputs from the reduce-order regression model that is trained offline. As an important part of *machine*
50 *learning* [5, 31], regression methods have been intensively developed in *supervised learning*. Among the
51 existing regression models, the proposed regression-based RB method employs a *Gaussian process regression*
52 (GPR), which infers that the observed input-output pairs follow a prior of Gaussian process, and then makes
53 predictions for new parameter values according to the posterior. Based on the work about a Gaussian
54 functional regression framework in [33, 34], the Gaussian-type regression was combined with the reduced
55 basis method in [35] to predict some quantities of interest of the high-fidelity simulation. In this work,
56 however, the GPR is employed to recover the full solution fields of the nonlinear problems. Equipped
57 with an active data selection for the training samples, the efficiency of the GPR can be further enhanced.
58 Numerical results also indicate that the GPR model shows good performance in both accuracy and efficiency
59 of ROM's for nonlinear structural analysis.

60 Following the introduction, the basic equations of nonlinear structural analysis are briefly reviewed in
61 Section 2. In Section 3, the regression-based RB method is presented and the procedure is specified. After an
62 introduction to the key ideas of GPR, application of GPR to the ROM for structural problems is addressed
63 in Section 4, with an active data selection algorithm proposed to enhance efficiency. In Section 5, the
64 method is tested and validated by two examples of large deformation analysis, one in 1D and the other in
65 3D. Finally, some conclusions are drawn in Section 6.

66 For the clarity of the notation, italic bold symbols are adopted in this paper for coordinates, vector fields
67 and tensor fields, such as coordinates \mathbf{X} , displacement vector field \mathbf{u} , strain tensor field \mathbf{E} and stress tensor
68 field \mathbf{S} ; and upright bold symbols are used for vectors and matrices in linear algebra, such as regression
69 input vector \mathbf{x} , collection of outputs \mathbf{y} , observed input matrix \mathbf{X} , discrete displacement solution \mathbf{u}_h and the
70 snapshot matrix \mathbf{S} .

2. Nonlinear structural analysis

2.1. Governing equations

In the following, a general deformable body is assumed to experience large deformation and a nonlinear constitutive response in a Cartesian coordinate system. The governing equations can be correspondingly given as follows:

$$\begin{aligned} \nabla_{\mathbf{X}} \cdot (\mathbf{F}(\mathbf{u})\mathbf{S}) + \mathbf{b} &= \mathbf{0} \quad \text{in } \Omega, \\ \mathbf{S} &= \mathbf{C}(\mathbf{E}(\mathbf{u})) \quad \text{in } \Omega, \\ \mathbf{u} &= \mathbf{0} \quad \text{on } \Gamma_D, \\ (\mathbf{F}(\mathbf{u})\mathbf{S})^T \hat{\mathbf{n}} &= \mathbf{t} \quad \text{on } \Gamma_N. \end{aligned} \tag{1}$$

Here the unknown $\mathbf{u} = \mathbf{u}(\mathbf{X})$ denotes the vector field of the displacement defined with respect to the original coordinates $\mathbf{X} \in \bar{\Omega}$ of the body, where $\bar{\Omega}$ is the undeformed configuration that the body occupies before the motion, and $\Omega \subset \mathbb{R}^3$ is the corresponding domain. The motion of the body is shown in Figure 1. Referred to as the *deformation gradient* tensor, the operator $\mathbf{F}(\cdot)$ is introduced as

$$\mathbf{F}(\mathbf{u}) = \mathbf{I} + \nabla_{\mathbf{X}}\mathbf{u}, \tag{2}$$

where \mathbf{I} is the unit tensor and $\nabla_{\mathbf{X}}$ is the gradient operator with respect to the original coordinates \mathbf{X} . The *Green-Lagrange strain* tensor field $\mathbf{E}(\cdot)$ is defined as the following nonlinear operator acting on the displacement field \mathbf{u} :

$$\mathbf{E}(\mathbf{u}) = \frac{1}{2} [\nabla_{\mathbf{X}}\mathbf{u} + (\nabla_{\mathbf{X}}\mathbf{u})^T + (\nabla_{\mathbf{X}}\mathbf{u})^T \nabla_{\mathbf{X}}\mathbf{u}]. \tag{3}$$

Moreover, \mathbf{S} denotes the *second Piola-Kirchhoff stress* field \mathbf{S} , which is usually used for large deformation analysis, \mathbf{b} is a prescribed body force applied on the structure with respect to the undeformed volume, \mathbf{t} is the prescribed traction with respect to the undeformed surface area and $\hat{\mathbf{n}}$ is the unit outward normal vector along Γ_N . The constitutive relation of the material can be expressed as a nonlinear operator \mathbf{C} which maps a tensor field of the Green-Lagrange strain to the corresponding tensor field of second Piola-Kirchhoff stresses.

In this work, two typical nonlinear constitutive relations in structural analysis, hyperelasticity and elastoplasticity, are considered. We refer to [7, 45] for more details about them and a variety of other constitutive relations. Moreover, it should be pointed out that only quasi-static problems are taken into account in this work, i.e. the problems are assumed to be time-independent.

Remark 1: In this paper, only problems with homogeneous Dirichlet boundary conditions are discussed, as problems with inhomogeneous Dirichlet boundary conditions $\mathbf{u} = \mathbf{u}_D$ on Γ_D can be transformed to the homogeneous case, i.e. one can define $\mathbf{w} = \mathbf{u} - \mathbf{p}$ with $\mathbf{p} \in [C^\infty(\bar{\Omega})]^3$ being a predefined function that satisfies the boundary conditions $\mathbf{p} = \mathbf{u}_D$ on Γ_D , and solve for \mathbf{w} by replacing \mathbf{u} with $\mathbf{w} + \mathbf{p}$ in the problem.

2.2. Nonlinear structural problems and their parametrization

Combining the governing equations in Subsection 2.1, one has the following weak formulation of a nonlinear structural problem, or referred to as the virtual work principle [3, 8]: find $\mathbf{u} \in \mathcal{V}$ such that

$$\int_{\Omega} \mathbf{C}(\mathbf{E}(\mathbf{u})) : D\mathbf{E}[\mathbf{u}](\mathbf{v}) \, d\Omega = \int_{\Omega} \mathbf{b}^T \mathbf{v} \, d\Omega + \int_{\Gamma_N} \mathbf{t}^T \mathbf{v} \, d\Gamma \quad \forall \mathbf{v} \in \mathcal{V}, \tag{4}$$

where $\mathcal{V} = \{\mathbf{v} : \bar{\Omega} \rightarrow \mathbb{R}^3 \text{ smooth enough, } \mathbf{v} = \mathbf{0} \text{ on } \Gamma_D\}$, and $D\mathbf{E}[\mathbf{u}](\mathbf{v})$ stands for the Gâteaux derivative of \mathbf{E} at \mathbf{u} in the direction \mathbf{v} and can be expressed explicitly as

$$D\mathbf{E}[\mathbf{u}](\mathbf{v}) = \frac{1}{2} [\nabla_{\mathbf{X}}\mathbf{v} + (\nabla_{\mathbf{X}}\mathbf{v})^T + (\nabla_{\mathbf{X}}\mathbf{v})^T \nabla_{\mathbf{X}}\mathbf{u} + (\nabla_{\mathbf{X}}\mathbf{u})^T \nabla_{\mathbf{X}}\mathbf{v}]. \tag{5}$$

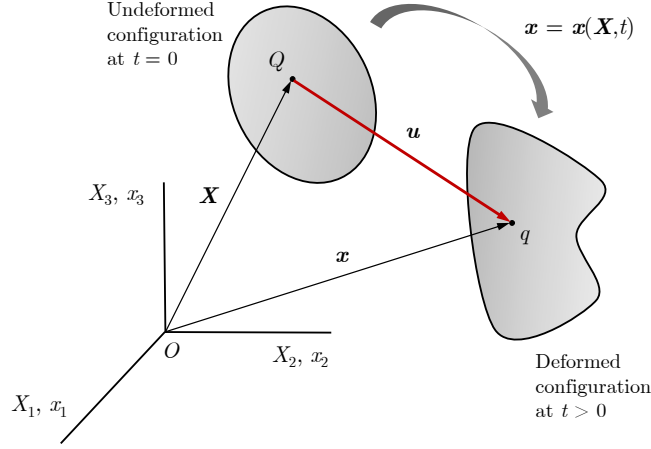


Figure 1: Motion of a deformable body

103 **Remark 2:** To ensure regularity, the solution \mathbf{u} to a nonlinear structural problem is considered to belong
 104 to Sobolev space $[W^{2,p}(\Omega)]^3$ with some $p > 3$, see [15] for example. In this paper, such considerations are
 105 irrelevant to the proposed reduced order modelling techniques, so the smoothness of solutions is merely
 106 described as 'smooth enough' for simplification.

107 Usually, finite elements are adopted to discretize the problem, translating it into finding a solution \mathbf{u}_h in
 108 a finite-dimensional space $\mathcal{V}_h \subset \mathcal{V}$. An incremental formulation is employed for applying external loads onto
 109 the structure. Within a loading increment, iterative algorithms, such as the Newton-Raphson algorithm and
 110 the arc-length method [3, 8], can be used to solve the nonlinear algebraic/discrete equations. In this work,
 111 the total Lagrangian formulation is used as an incremental formulation, in which the discrete equations are
 112 formulated and updated with respect to the undeformed configuration.

113 Furthermore, physical parametrization is taken into account in this paper. Several parameters are
 114 considered for some characteristics in the constitutive relation and the external loads. Then the parametrized
 115 nonlinear problem, corresponding to (4), is given as: for any given parameter $\boldsymbol{\mu} \in \mathcal{P} \subset \mathbb{R}^d$,

$$\int_{\Omega} \mathcal{C}(\mathbf{E}(\mathbf{u}(\boldsymbol{\mu})); \boldsymbol{\mu}) : D\mathbf{E}[\mathbf{u}(\boldsymbol{\mu})](\mathbf{v}) \, d\Omega = \int_{\Omega} \mathbf{b}(\boldsymbol{\mu})^T \mathbf{v} \, d\Omega + \int_{\Gamma_N} \mathbf{t}(\boldsymbol{\mu})^T \mathbf{v} \, d\Gamma \quad \forall \mathbf{v} \in \mathcal{V}, \quad (6)$$

116 where \mathcal{P} is the parameter domain and d is the total number of parameters. For cases with parameters in
 117 the geometry, [22, 28] can be referred to for details. After a transformation to the parameter-independent
 118 reference domain, the treatment will be similar to the strategy for physical parameters.

119 3. The reduced basis method for nonlinear structural analysis

120 Due to the use of an incremental formulation and iteration algorithms, solving the parametrized nonlinear
 121 problem (6) by a finite element discretization requires the assembly and solution of a number of linear
 122 systems. The dimension of such linear systems, denoted by N_h and referred to as the number of degrees
 123 of freedom (DOFs), is determined by both the underlying mesh and the polynomial order that the finite
 124 element analysis employs. The high-fidelity solution to a real-world structural problem often requires a
 125 large number of DOFs and many steps of increments and iterations, implying that the full-order model is
 126 expensive. Thus a direct numerical approximation of the full-order model is not affordable in many-query
 127 or real-time context of parametrized nonlinear structural analysis.

128 The reduced basis (RB) method is proposed as an efficient and convenient tool for model order reduction.
 129 It seeks the approximate solution to a parameterized problem in a reduced space spanned by a set of

parameter-independent RB functions, constructed from a collection of high-fidelity snapshots at different parameter values. The RB functions are either carefully chosen from the snapshots by the Greedy algorithm [13, 37, 41], or by principal ingredient analysis of snapshots. The former requires an error estimator/indicator for the full-order solution, and picks the snapshot that maximizes the estimator/indicator as a new RB function until a criteria is satisfied. However, proper error estimators or indicators for a general nonlinear structural problem are unknown, so the latter approach is utilized with the aid of the proper orthogonal decomposition (POD) [20, 26, 38], as detailed in the following.

To evaluate the reduced-order solution for any desired value in the parameter domain, a regression-based approach will be introduced to parametrized nonlinear structural analysis, rather than the conventional Galerkin-projection-based approach.

3.1. Full-order solutions and snapshots

The notion of a solution manifold can be introduced, comprising all the solutions of the parametrized problem (6) under variation of the parameters, i.e. $\mathcal{M} = \{\mathbf{u}(\boldsymbol{\mu}) : \boldsymbol{\mu} \in \mathcal{P}\} \subset \mathcal{V}$. Since the exact solutions are not available, a discrete counterpart of \mathcal{M} can be considered as $\mathcal{M}_h = \{\mathbf{u}_h(\boldsymbol{\mu}) : \boldsymbol{\mu} \in \mathcal{P}\} \subset \mathcal{V}_h$, where $\mathbf{u}_h(\boldsymbol{\mu})$ is the high-fidelity full-order solution obtained by finite element analysis, i.e. $\mathbf{u}_h(\mathbf{X}; \boldsymbol{\mu}) = \sum_{i=1}^{N_h} (\mathbf{u}_h(\boldsymbol{\mu}))_i \phi_i(\mathbf{X})$. Here N_h is the number of DOFs, $\mathbf{u}_h(\boldsymbol{\mu})$ is an N_h -dimensional vector collecting all the values of the DOFs, and ϕ_i is the i th basis/shape function. Note that the finite element space \mathcal{V}_h is spanned by all the shape functions, i.e. $\mathcal{V}_h = \text{span}\{\phi_1, \phi_2, \dots, \phi_{N_h}\}$. The discrete solution $\mathbf{u}_h(\boldsymbol{\mu})$ for any parameter $\boldsymbol{\mu}$ is calculated under a fixed finite element setting.

To generate an RB space for the nonlinear problem, one considers a collection of N_s snapshots $\{\mathbf{u}_h(\boldsymbol{\mu}^1), \mathbf{u}_h(\boldsymbol{\mu}^2), \dots, \mathbf{u}_h(\boldsymbol{\mu}^{N_s})\}$ associated with a discrete point-set $\Theta = \{\boldsymbol{\mu}^1, \boldsymbol{\mu}^2, \dots, \boldsymbol{\mu}^{N_s}\} \subset \mathcal{P}$ in the parameter domain. Then a subspace of \mathcal{V}_h can be spanned by the snapshots as

$$\mathcal{M}_\Theta = \text{span}\{\mathbf{u}_h(\boldsymbol{\mu}^1), \mathbf{u}_h(\boldsymbol{\mu}^2), \dots, \mathbf{u}_h(\boldsymbol{\mu}^{N_s})\} \subset \mathcal{V}_h. \quad (7)$$

The discrete point-set Θ is either a uniform lattice or a collection of generated points over the parameter domain \mathcal{P} . If Θ is fine enough, \mathcal{M}_Θ can act as a good representation of \mathcal{M}_h .

To reduce the model, a low-rank approximation \mathcal{V}_{rb} with rank $L \ll \min\{N_h, N_s\}$ should be found for \mathcal{M}_Θ . Towards this end, the POD is employed in this work to extract RB functions $\{\boldsymbol{\psi}_1, \boldsymbol{\psi}_2, \dots, \boldsymbol{\psi}_L\}$ from snapshots and then span the RB space \mathcal{V}_{rb} as

$$\mathcal{V}_{\text{rb}} = \text{span}\{\boldsymbol{\psi}_1, \boldsymbol{\psi}_2, \dots, \boldsymbol{\psi}_L\}, \quad (8)$$

as detailed in next subsection.

3.2. The proper orthogonal decomposition and the reduced basis space

Consider a *snapshot matrix* $\mathbf{S} \in \mathbb{R}^{N_h \times N_s}$ collecting the DOFs of all snapshots, i.e

$$\mathbf{S} = [\mathbf{u}_h(\boldsymbol{\mu}^1) \mid \mathbf{u}_h(\boldsymbol{\mu}^2) \mid \dots \mid \mathbf{u}_h(\boldsymbol{\mu}^{N_s})]. \quad (9)$$

In the context of nonlinear structural analysis, it is assumed that the number of snapshots is less than that of DOFs, i.e. $N_s \ll N_h$, to avoid a high cost of preparing full-order snapshots.

The POD takes advantage of the *singular value decomposition* (SVD) of matrix \mathbf{S} , given as

$$\mathbf{S} = \mathbf{U}\boldsymbol{\Sigma}\mathbf{Z}^T \quad (10)$$

with $\mathbf{U} \in \mathbb{R}^{N_h \times N_h}$ and $\mathbf{Z} \in \mathbb{R}^{N_s \times N_s}$ being orthogonal matrices, i.e. $\mathbf{U}^T \mathbf{U} = \mathbf{I}_{N_h}$ and $\mathbf{Z}^T \mathbf{Z} = \mathbf{I}_{N_s}$, and $\boldsymbol{\Sigma} = \text{diag}\{\sigma_1, \sigma_2, \dots, \sigma_{N_s}\}$ containing the singular values $\sigma_1 \geq \sigma_2 \geq \dots \geq \sigma_{N_s} \geq 0$.

Defined as a subspace of \mathbb{R}^{N_h} spanned by all the N_s columns of $\mathbf{S} \in \mathbb{R}^{N_h \times N_s}$, the column space of \mathbf{S} is denoted by $\text{Col}(\mathbf{S})$. At the algebraic level, one seeks to find the 'best' approximation of $\text{Col}(\mathbf{S})$, in some optimal sense, among all L -dimensional subspaces with $L \leq \text{rank}(\mathbf{S})$. Let $\mathbf{V} \in \mathbb{R}^{N_h \times L}$ denote the first L columns of \mathbf{U} , and let $\mathbb{Y}_L = \{\mathbf{W} \in \mathbb{R}^{N_h \times L} : \mathbf{W}^T \mathbf{W} = \mathbf{I}_L\}$ represent the set of all L -dimensional orthogonal

169 bases. The projection error of snapshots onto orthogonal bases $\mathbf{W} \in \mathbb{Y}_L$ in the Euclidean norm can be
 170 expressed as $\sum_{i=1}^{N_s} \|\mathbf{u}_h(\boldsymbol{\mu}^i) - \mathbf{W}\mathbf{W}^T \mathbf{u}_h(\boldsymbol{\mu}^i)\|_{\mathbb{R}^{N_h}}^2$.

171 The Schmidt-Eckart-Young theorem [17, 38, 42] states that the basis consisting of the first L left singular
 172 vectors of \mathbf{S} minimizes the projection error of snapshots among all the L -dimensional orthogonal bases in
 173 \mathbb{R}^{N_h} , and the error can be evaluated by the $(L+1)$ th to N_s th singular values, i.e.

$$\sum_{i=1}^{N_s} \left\| \mathbf{u}_h(\boldsymbol{\mu}^i) - \mathbf{V}\mathbf{V}^T \mathbf{u}_h(\boldsymbol{\mu}^i) \right\|_{\mathbb{R}^{N_h}}^2 = \min_{\mathbf{W} \in \mathbb{Y}_L} \sum_{i=1}^{N_s} \left\| \mathbf{u}_h(\boldsymbol{\mu}^i) - \mathbf{W}\mathbf{W}^T \mathbf{u}_h(\boldsymbol{\mu}^i) \right\|_{\mathbb{R}^{N_h}}^2 = \sum_{i=L+1}^{N_s} \sigma_i^2. \quad (11)$$

174 Thus one obtains that $\text{Col}(\mathbf{S})$ can be well approximated by $\text{Col}(\mathbf{V})$ with a small L if the singular values
 175 decay rapidly.

176 The procedure of the POD is then given as the following algorithm:

Algorithm 1 POD

Input: Snapshot matrix \mathbf{S} , projection error tolerance ϵ_{POD}

Output: Reduced rank L , matrix \mathbf{V} collecting the RB

- 1: Form the correlation matrix $\mathbf{M} = \mathbf{S}^T \mathbf{S} \in \mathbb{R}^{N_s \times N_s}$;
 - 2: Solve the eigenvalue problem for \mathbf{M} , i.e. $\mathbf{M}\mathbf{x}_i = \sigma_i^2 \mathbf{x}_i$, $i = 1, 2, \dots, N_s$;
 - 3: Set $\mathbf{v}_i = \frac{1}{\sigma_i} \mathbf{S}\mathbf{x}_i$, $i = 1, 2, \dots, \text{rank}(\mathbf{S})$;
 - 4: Define $L \leq \text{rank}(\mathbf{S})$ as the minimum integer s.t. $\frac{\sum_{i=1}^L \sigma_i^2}{\sum_{i=1}^{N_s} \sigma_i^2} > 1 - \epsilon_{\text{POD}}$;
 - 5: Define $\mathbf{V} = [\mathbf{v}_1 \mid \mathbf{v}_2 \mid \dots \mid \mathbf{v}_L]$.
-

177 The desired rank L can also be defined directly, rather than determined by the tolerance ϵ_{POD} .

178 Corresponding to the approximation of $\text{Col}(\mathbf{S})$ by $\text{Col}(\mathbf{V})$ on the algebraic level, function space \mathcal{M}_Θ is
 179 hence approximated by $\mathcal{V}_{\text{rb}} = \text{span}\{\boldsymbol{\psi}_1, \boldsymbol{\psi}_2, \dots, \boldsymbol{\psi}_L\}$ with the RB functions $\boldsymbol{\psi}_l$ defined as $\boldsymbol{\psi}_l = \sum_{k=1}^{N_h} V_{kl} \boldsymbol{\phi}_k$,
 180 $l = 1, 2, \dots, L$. It is noticed that there exists a biunique correspondence between the elements in \mathcal{V}_{rb} and
 181 those in $\text{Col}(\mathbf{V})$, i.e. for any $\mathbf{w}_L \in \mathbb{R}^L$

$$\mathbf{w}_{\text{rb}} := \mathbf{V}\mathbf{w}_L \in \text{Col}(\mathbf{V}) \quad \Leftrightarrow \quad \mathbf{w}_{\text{rb}} = \sum_{k=1}^{N_h} (\mathbf{w}_{\text{rb}})_k \boldsymbol{\phi}_k = \sum_{l=1}^L (\mathbf{w}_L)_l \boldsymbol{\psi}_l \in \mathcal{V}_{\text{rb}}. \quad (12)$$

3.3. Regression-based approach for reduced-order solutions

182 The numerical procedure of the RB method is efficiently carried out in an *offline-online* framework.
 183 As discussed, the RB functions are prepared from the high-fidelity snapshots in the parameter-independent
 184 offline stage. The reduced-order solution for a new parameter is then sought in the online stage. The
 185 Galerkin-projection-based approach is the most often used for this, i.e. the problem for a new parameter
 186 value is solved in the RB space \mathcal{V}_{rb} by a standard Galerkin approach.

187 However, the Galerkin-projection-based scheme will not significantly save computational cost for a general
 188 nonlinear structural problem. In addition to compromising the efficiency due to the non-affinity in parameter
 189 dependence, the structural configuration and matrix assembly have to be updated during all the loading
 190 increments and iterations when solving nonlinear algebraic equations. Moreover, there may exist convergence
 191 or updating issues in some complex cases due to the possibility that some configurations in the incremental
 192 procedure are not represented well in \mathcal{V}_{rb} .

193 Therefore, a regression-based approach is proposed to calculate reduced-order solutions for new pa-
 194 rameters. In this scenario, the projection of a full-order discrete solution $\mathbf{u}_h(\boldsymbol{\mu})$ onto $\text{Col}(\mathbf{V})$ acts as the
 195 corresponding reduced-order solution at algebraic level,
 196

$$\mathbf{u}_{\text{rb}}(\boldsymbol{\mu}) = \mathbf{V}\mathbf{V}^T \mathbf{u}_h(\boldsymbol{\mu}) = \arg \min_{\mathbf{w}_h \in \text{Col}(\mathbf{V})} \|\mathbf{u}_h(\boldsymbol{\mu}) - \mathbf{w}_h\|_{\mathbb{R}^{N_h}}, \quad (13)$$

197 in which $\mathbf{V}^T \mathbf{u}_h(\boldsymbol{\mu}) = \mathbf{u}_L(\boldsymbol{\mu})$ collects the coefficients associated with column bases of \mathbf{V} .

198 To obtain the projection coefficients $\mathbf{u}_L(\boldsymbol{\mu})$ for any desired parameter $\boldsymbol{\mu} \in \mathcal{P}$, one can resort to a nonlinear
199 regression $\hat{\boldsymbol{\pi}}$ between $d = \dim(\mathcal{P})$ inputs and L outputs:

$$\boldsymbol{\mu} \mapsto \mathbf{u}_L(\boldsymbol{\mu}) = \mathbf{V}^T \mathbf{u}_h(\boldsymbol{\mu}) \approx \hat{\boldsymbol{\pi}}(\boldsymbol{\mu}). \quad (14)$$

200 This regression model $\hat{\boldsymbol{\pi}}(\cdot)$ should be constructed from a set of training data $\mathcal{D} = \{(\boldsymbol{\mu}_i, \mathbf{V}^T \mathbf{u}_h(\boldsymbol{\mu}_i)) : i =$
201 $1, 2, \dots, M\}$ during the offline stage, where $\mathbf{u}_h(\boldsymbol{\mu}_i)$ is the full-order solution for each sample. The model is
202 used during the online stage to recover the output $\hat{\boldsymbol{\pi}}(\boldsymbol{\mu}^*)$ for any new input $\boldsymbol{\mu}^* \in \mathcal{P}$. Correspondingly, the
203 reduced-order solution $\mathbf{u}_{\text{rb,reg}}(\boldsymbol{\mu}^*) \in \mathcal{V}_{\text{rb}}$ is given as

$$\mathbf{u}_{\text{rb,reg}}(\boldsymbol{\mu}^*) = \sum_{l=1}^L (\hat{\boldsymbol{\pi}}(\boldsymbol{\mu}^*))_l \boldsymbol{\psi}_l = \sum_{k=1}^{N_h} (\mathbf{V} \hat{\boldsymbol{\pi}}(\boldsymbol{\mu}^*))_k \boldsymbol{\phi}_k = \sum_{k=1}^{N_h} (\mathbf{u}_{\text{rb,reg}}(\boldsymbol{\mu}^*))_k \boldsymbol{\phi}_k, \quad (15)$$

204 where $\mathbf{V} \hat{\boldsymbol{\pi}}(\boldsymbol{\mu}^*) = \mathbf{u}_{\text{rb,reg}}(\boldsymbol{\mu}^*)$ recovers the nodal values of the solution. Once the regression model is obtained,
205 the online stage only requires direct outputs from this model, ensuring that the online computation is carried
206 out at low cost.

Algorithm 2 Regression-based RB method for nonlinear structural analysis (algebraic level)

1: **Offline stage:**

2: Compute N_s full-order snapshots $\{\mathbf{u}_h(\boldsymbol{\mu}^1), \mathbf{u}_h(\boldsymbol{\mu}^2), \dots, \mathbf{u}_h(\boldsymbol{\mu}^{N_s})\}$ and form the snapshot matrix $\mathbf{S} \in$
 $\mathbb{R}^{N_h \times N_s}$;

3: Perform POD for \mathbf{S} and get the L orthogonal bases $\mathbf{V} \in \mathbb{R}^{N_h \times L}$;

4: Prepare the training set $\mathcal{D} = \{(\boldsymbol{\mu}_i, \mathbf{V}^T \mathbf{u}_h(\boldsymbol{\mu}_i)) : i = 1, 2, \dots, M\}$;

5: Construct the regression model $\hat{\boldsymbol{\pi}}(\cdot)$ from \mathcal{D} .

6: **Online stage:**

7: Recover output $\hat{\boldsymbol{\pi}}(\boldsymbol{\mu}^*)$ for a new parameter value $\boldsymbol{\mu}^*$;

8: Evaluate the reduced-order solution $\mathbf{u}_{\text{rb,reg}}(\boldsymbol{\mu}^*) = \sum_{k=1}^{N_h} (\mathbf{V} \hat{\boldsymbol{\pi}}(\boldsymbol{\mu}^*))_k \boldsymbol{\phi}_k$.

207 **Remark 3:** In some cases, the snapshots for the construction of the RB space can be included into the
208 training set and reused as training samples.

209 We note the complete decoupling of online and offline stages, and the non-intrusive nature of the
210 regression-based RB method. A Gaussian process model is utilized to construct the regression $\hat{\boldsymbol{\pi}}(\cdot)$, as
211 discussed in the following section.

212 4. Gaussian process regression model

213 In supervised learning, regression is concerned with prediction of continuous quantities of interest by
214 constructing a model from a set of observation data. Let $\mathcal{D} = \{(\mathbf{x}_i, y_i) : i = 1, 2, \dots, M\}$ denote the
215 training set of M observations, where each input $\mathbf{x}_i \in \mathcal{P} \subset \mathbb{R}^d$ consists of d entries and lies in the input
216 domain \mathcal{P} , and y_i is the output corresponding to \mathbf{x}_i . In a Gaussian process regression (GPR) model [40, 46],
217 the observed input-output pairs are assumed to follow some unknown regression function $f : \mathcal{P} \rightarrow \mathbb{R}$ as
218 $y_i = f(\mathbf{x}_i)$, possibly corrupted by noise. The model then infers a probabilistic distribution over functions
219 given the data, and uses this distribution to make predictions when given new inputs.

220 4.1. Gaussian processes for regression

221 A Gaussian process (GP) is a collection of random variables, any finite number of which obeys a joint
222 Gaussian distribution. In the case of GPR, let the prior on the regression function be a GP corrupted by

223 an independent Gaussian noise term, i.e. for $(\mathbf{x}, \mathbf{x}') \in \mathcal{P} \times \mathcal{P}$,

$$f(\mathbf{x}) \sim \text{GP}(0, \kappa(\mathbf{x}, \mathbf{x}')), \quad y = f(\mathbf{x}) + \epsilon, \quad \epsilon \sim \mathcal{N}(0, \sigma_y^2). \quad (16)$$

224 There are many different choices for the covariance function $\kappa : \mathcal{P} \times \mathcal{P} \rightarrow \mathbb{R}$. A frequently used one is the
225 *squared exponential* (SE) *kernel*:

$$\kappa(\mathbf{x}, \mathbf{x}') = \sigma_f^2 \exp\left(-\frac{1}{2\ell^2} \|\mathbf{x} - \mathbf{x}'\|_{\mathbb{R}^d}^2\right), \quad (17)$$

226 containing two hyperparameters: the standard deviation parameter σ_f and the correlated lengthscale ℓ .
227 Another covariance function, that we will use in this work, is the *automatic relevance determination* (ARD)
228 SE kernel:

$$\kappa(\mathbf{x}, \mathbf{x}') = \sigma_f^2 \exp\left(-\frac{1}{2} \sum_{m=1}^d \frac{(x_m - x'_m)^2}{\ell_m^2}\right), \quad (18)$$

229 which considers an individual correlated lengthscale for each input dimension, and allows for differentiated
230 relevances of input features to the regression.

231 Given a finite number of points in the input domain, a prior joint Gaussian is thus defined for the
232 regression outputs:

$$\mathbf{y}|\mathbf{X} \sim \mathcal{N}(\mathbf{0}, \mathbf{K}_y), \quad \mathbf{K}_y = \text{cov}[\mathbf{y}|\mathbf{X}] = \kappa(\mathbf{X}, \mathbf{X}) + \sigma_y^2 \mathbf{I}_M, \quad (19)$$

233 where $\mathbf{y} = \{y_1, y_2, \dots, y_M\}^\top$, $\mathbf{X} = [\mathbf{x}_1 | \mathbf{x}_2 | \dots | \mathbf{x}_M]$ and \mathbf{I}_M is the M -dimensional unit matrix.

234 Given a set of M^* new test inputs denoted by $\mathbf{X}^* \in \mathbb{R}^{d \times M^*}$, predictions of the corresponding noise-
235 free outputs $\mathbf{f}^* \in \mathbb{R}^{M^*}$ are desired. From the joint density of the observed outputs \mathbf{y} and the noise-free
236 test outputs \mathbf{f}^* , the standard rules for conditioning Gaussians gives the posterior predictive distribution for
237 $\mathbf{f}^* \in \mathbb{R}^{M^*}$ as follows

$$\begin{aligned} \mathbf{f}^*|\mathbf{X}^*, \mathbf{X}, \mathbf{y} &\sim \mathcal{N}(\mathbf{m}^*, \mathbf{C}^*), \\ \mathbf{m}^* &= \mathbf{K}^{*\top} \mathbf{K}_y^{-1} \mathbf{y}, \quad \mathbf{C}^* = \mathbf{K}^{**} - \mathbf{K}^{*\top} \mathbf{K}_y^{-1} \mathbf{K}^*, \end{aligned} \quad (20)$$

238 where $\mathbf{K}^{**} = \kappa(\mathbf{X}^*, \mathbf{X}^*)$ and $\mathbf{K}^* = \kappa(\mathbf{X}^*, \mathbf{X})$.

239 The values of the hyperparameters $\boldsymbol{\theta}$ make significant difference on the predictive performance, with
240 $\boldsymbol{\theta} = \{\sigma_f, \ell, \sigma_y\}$ for the case of SE kernel and $\boldsymbol{\theta} = \{\sigma_f, \ell_1, \dots, \ell_d, \sigma_y\}$ for the case of ARD SE kernel.
241 In this work, an empirical Bayesian approach of maximizing likelihood is adopted to determine a set of
242 optimal values of the parameters. Using a standard gradient-based optimizer, one can estimate the optimal
243 hyperparameters $\boldsymbol{\theta}_{\text{opt}}$ via the maximization problem:

$$\boldsymbol{\theta}_{\text{opt}} = \arg \max_{\boldsymbol{\theta}} \log p(\mathbf{y}|\mathbf{X}) = \arg \max_{\boldsymbol{\theta}} \left\{ -\frac{1}{2} \mathbf{y}^\top \mathbf{K}_y^{-1}(\boldsymbol{\theta}) \mathbf{y} - \frac{1}{2} \log |\mathbf{K}_y(\boldsymbol{\theta})| - \frac{M}{2} \log(2\pi) \right\}, \quad (21)$$

244 where $p(\mathbf{y}|\mathbf{X})$ is the conditional density function of \mathbf{y} given \mathbf{X} , also considered as the marginal likelihood.

245 The procedure of a GPR is given as the following algorithm.

Algorithm 3 GPR

Input: A training set of M observations $\mathcal{D} = \{(\mathbf{x}_i, y_i) : i = 1, 2, \dots, M\}$, a chosen kernel function $\kappa(\cdot, \cdot)$, test inputs $\mathbf{X}^* \in \mathbb{R}^{d \times M^*}$

Output: Test outputs $\mathbf{f}^* | \mathbf{X}^*, \mathbf{X}, \mathbf{y}$

- 1: Estimate the optimal hyperparameters $\boldsymbol{\theta}_{\text{opt}}$ by maximizing the likelihood, in each iterative step of which one needs to
 - 2: Form a covariance matrix $\mathbf{K}_y = \kappa(\mathbf{X}, \mathbf{X}) + \sigma_y^2 \mathbf{I}_M$;
 - 3: Calculate a vector $\mathbf{a} \in \mathbb{R}^M$ such that $\mathbf{K}_y \mathbf{a} = \mathbf{y}$;
 - 4: Calculate the likelihood $\log p(\mathbf{y} | \mathbf{X}) = -\frac{1}{2} \mathbf{y}^T \mathbf{a} - \frac{1}{2} \log |\mathbf{K}_y| - \frac{M}{2} \log(2\pi)$;
 - 5: Calculate the gradient of the likelihood with respect to the hyperparameters;
 - 6: Set $\mathbf{K}_y = \mathbf{K}_y(\boldsymbol{\theta}_{\text{opt}})$ and $\mathbf{a} = \mathbf{a}(\boldsymbol{\theta}_{\text{opt}})$ for the optimal hyperparameters;
 - 7: Form correlation matrices $\mathbf{K}^{**} = \kappa(\mathbf{X}^*, \mathbf{X}^*)$ and $\mathbf{K}^* = \kappa(\mathbf{X}^*, \mathbf{X})$ for the optimal hyperparameters;
 - 8: Calculate a matrix $\mathbf{A}^* \in \mathbb{R}^{M \times M^*}$ such that $\mathbf{K}_y \mathbf{A}^* = \mathbf{K}^*$;
 - 9: Form the conditioning mean value vector $\mathbf{m}^* = \mathbf{K}^{*T} \mathbf{a}$ and the corresponding covariance matrix $\mathbf{C}^* = \mathbf{K}^{**} - \mathbf{K}^{*T} \mathbf{A}^*$;
 - 10: Define $\mathbf{f}^* | \mathbf{X}^*, \mathbf{X}, \mathbf{y} \sim \mathcal{N}(\mathbf{m}^*, \mathbf{C}^*)$.
-

4.2. Gaussian process regression for the reduced basis method of nonlinear structural analysis

As already mentioned in Section 3, the GPR is utilized in the RB method for nonlinear structural analysis. A GP regression model $\hat{\boldsymbol{\pi}}_{\text{GP}} : \mathcal{P} \rightarrow \mathbb{R}^L$ is constructed for the mapping $\boldsymbol{\mu} \mapsto \mathbf{V}^T \mathbf{u}_h(\boldsymbol{\mu})$.

For the l th of L entries of $\hat{\boldsymbol{\pi}}_{\text{GP}}(\cdot)$, $1 \leq l \leq L$, the training data is set as $\mathbf{x}_i^l = \boldsymbol{\mu}_i$, $y_i^l = \mathbf{v}_l^T \mathbf{u}_h(\boldsymbol{\mu}_i)$ and $\mathcal{D}^l = \{(\mathbf{x}_i^l, y_i^l) : i = 1, 2, \dots, M\}$ for a GPR model, with \mathbf{v}_l being the l th column of \mathbf{V} . For a new parameter $\mathbf{x}^* = \boldsymbol{\mu}^* \in \mathcal{P}$ as test input, the corresponding output $\hat{\boldsymbol{\pi}}_{\text{GP}}(\boldsymbol{\mu}^*)$ consists of L independent Gaussian distributions, i.e.

$$(\hat{\boldsymbol{\pi}}_{\text{GP}}(\boldsymbol{\mu}^*))_l | \mathbf{X}^l, \mathbf{y}^l \sim \mathcal{N}(\mathbf{m}^{l*}, \mathbf{C}^{l*}), \quad l = 1, 2, \dots, L, \quad (22)$$

where $\mathbf{X}^l = [\mathbf{x}_1^l | \mathbf{x}_2^l | \dots | \mathbf{x}_M^l]$, $\mathbf{y}^l = \{y_1^l, y_2^l, \dots, y_M^l\}^T$, \mathbf{m}^{l*} and \mathbf{C}^{l*} for the l th entry of $\hat{\boldsymbol{\pi}}_{\text{GP}}(\cdot)$ are defined in the same way as \mathbf{m}^* and \mathbf{C}^* in (20). Correspondingly, the reduced-order discrete solution $\tilde{\mathbf{u}}_{\text{rb,GPR}}(\boldsymbol{\mu}^*)$ collects N_h Gaussian distributions, i.e.

$$\tilde{\mathbf{u}}_{\text{rb,GPR}}(\boldsymbol{\mu}^*) = \mathbf{V} \hat{\boldsymbol{\pi}}_{\text{GP}}(\boldsymbol{\mu}^*). \quad (23)$$

The reduced order solution, expressed as a random field over Ω , is given as

$$\tilde{\mathbf{u}}_{\text{rb,GPR}}(\boldsymbol{\mu}^*) = \sum_{l=1}^L (\hat{\boldsymbol{\pi}}_{\text{GP}}(\boldsymbol{\mu}^*))_l \boldsymbol{\psi}_l = \sum_{k=1}^{N_h} (\mathbf{V} \hat{\boldsymbol{\pi}}_{\text{GP}}(\boldsymbol{\mu}^*))_k \boldsymbol{\phi}_k = \sum_{k=1}^{N_h} (\tilde{\mathbf{u}}_{\text{rb,GPR}}(\boldsymbol{\mu}^*))_k \boldsymbol{\phi}_k. \quad (24)$$

For a set of r test samples $\mathcal{T} = \{(\boldsymbol{\mu}_i^*, \mathbf{u}_h(\boldsymbol{\mu}_i^*)) : i = 1, 2, \dots, r\}$, $\boldsymbol{\mu}_i^*$ being the i th test input and $\mathbf{u}_h(\boldsymbol{\mu}_i^*)$ being the corresponding full-order discrete solution, an average relative error for GPR predictions can be defined as

$$\bar{\epsilon}_t(\mathcal{T}) = \frac{1}{r} \sum_{i=1}^r \frac{\|\mathbf{u}_h(\boldsymbol{\mu}_i^*) - \mathbb{E}[\tilde{\mathbf{u}}_{\text{rb,GPR}}(\boldsymbol{\mu}_i^*)]\|_{\mathbb{R}^{N_h}}}{\|\mathbf{u}_h(\boldsymbol{\mu}_i^*)\|_{\mathbb{R}^{N_h}}} = \frac{1}{r} \sum_{i=1}^r \frac{\|\mathbf{u}_h(\boldsymbol{\mu}_i^*) - \mathbf{V} \mathbb{E}[\hat{\boldsymbol{\pi}}_{\text{GP}}(\boldsymbol{\mu}_i^*)]\|_{\mathbb{R}^{N_h}}}{\|\mathbf{u}_h(\boldsymbol{\mu}_i^*)\|_{\mathbb{R}^{N_h}}}, \quad (25)$$

note that the mean values of GPR test outputs are considered as predictions.

Remark 4: In the context of structural optimization, reliability analysis, etc., gradient-based algorithms are used for solving optimization problems, see [14, 18, 29]. These algorithms usually require the derivatives of the structural responses with respect to the parameters. In (20), the mean value of GPR output $m^*(\mathbf{x}^*) = \mathbb{E}[f(\mathbf{x}^*) | \mathbf{X}, \mathbf{y}]$ for a new test parameter \mathbf{x}^* is obtained as

$$m^*(\mathbf{x}^*) = \kappa(\mathbf{x}^*, \mathbf{X})^T \mathbf{K}_y^{-1} \mathbf{y}. \quad (26)$$

265 Correspondingly, the derivative of m^* with respect to \mathbf{x}^* is thus derived as

$$\frac{\partial m^*(\mathbf{x}^*)}{\partial \mathbf{x}^*} = \left[\frac{\partial \kappa(\mathbf{x}^*, \mathbf{X})}{\partial \mathbf{x}^*} \right]^T \mathbf{K}_y^{-1} \mathbf{y}, \quad (27)$$

266 which only depends on the parameter location \mathbf{x}^* and is not correlated to any other test points. For a
 267 nonlinear structural problem, the derivative of test output $\mathbb{E}[\hat{\boldsymbol{\pi}}_{\text{GP}}(\boldsymbol{\mu}^*)]$ can be calculated for test input $\boldsymbol{\mu}^*$,
 268 entry by entry, and the response sensitivity derivative expressed as

$$\frac{\partial}{\partial \boldsymbol{\mu}^*} \tilde{\mathbf{u}}_{\text{rb,GPR}}(\boldsymbol{\mu}^*) = \mathbf{V} \frac{\partial}{\partial \boldsymbol{\mu}^*} \mathbb{E}[\hat{\boldsymbol{\pi}}_{\text{GP}}(\boldsymbol{\mu}^*)]. \quad (28)$$

269 4.3. Active data selection for training samples

270 In the training set \mathcal{D} , each input-output pair $(\boldsymbol{\mu}_i, \mathbf{V}^T \mathbf{u}_h(\boldsymbol{\mu}_i))$ requires the calculation of full-order solu-
 271 tion $\mathbf{u}_h(\boldsymbol{\mu}_i)$ at parameter $\boldsymbol{\mu}_i$, $i = 1, 2, \dots, M$. A large number of training samples M implies substantial
 272 computation to prepare the training data. For efficiency, one should choose a set of 'optimal' training
 273 samples from a pool of parameters, so the full-order solutions are only calculated at a smaller number of
 274 optimized parameter values without substantial loss of accuracy. Referred to as *active data selection*, this
 275 type of selecting technique has been studied and developed in the field of *active learning* [16, 23, 27, 43, 44].

276 In the context of GPR model for nonlinear structural analysis, an active data selection algorithm is given
 277 as follows, analogous to a scheme of active learning [4, 44].

Algorithm 4 Selection algorithm for active training data

Input: A parameter pool $\mathcal{P}_s \subset \mathcal{P}$ with a large number of elements – uniform lattice or generated in \mathcal{P} ,
 $\boldsymbol{\mu}_1 \in \mathcal{P}_s$, tolerance tol , $M = 1$, training set $\mathcal{D} = \emptyset$ and active parameter set $\mathcal{P}_{tr} = \{\boldsymbol{\mu}_1\}$, test samples
 $\mathcal{T} = \{(\boldsymbol{\mu}_i^*, \mathbf{u}_h(\boldsymbol{\mu}_i^*)) : i = 1, 2, \dots, r\}$ with full-order solutions

Output: GPR model $\hat{\boldsymbol{\pi}}_{\text{GP}}(\cdot)$

- 1: Calculate full-order solution $\mathbf{u}_h(\boldsymbol{\mu}_M)$;
 - 2: Set $\mathcal{D} = \mathcal{D} \cup \{(\boldsymbol{\mu}_M, \mathbf{V}^T \mathbf{u}_h(\boldsymbol{\mu}_M))\}$;
 - 3: Train a GPR model $\hat{\boldsymbol{\pi}}_{\text{GP}}(\cdot)$ based on \mathcal{D} ;
 - 4: Calculate average relative error for test samples $\bar{\epsilon}_t(\mathcal{T})$;
 - 5: **if** $\bar{\epsilon}_t(\mathcal{T}) \leq \text{tol}$ **then**
 - 6: **Terminate**;
 - 7: **else**
 - 8: Update the parameter pool $\mathcal{P}_s = \mathcal{P}_s \setminus \mathcal{P}_{tr}$;
 - 9: **for each** $\boldsymbol{\mu} \in \mathcal{P}_s$ **do**
 - 10: Compute the output $\hat{\boldsymbol{\pi}}_{\text{GP}}(\boldsymbol{\mu})$;
 - 11: Evaluate the error indicator $\eta(\boldsymbol{\mu})$;
 - 12: **end for**
 - 13: Choose $\boldsymbol{\mu}_{M+1} = \arg \max_{\boldsymbol{\mu} \in \mathcal{P}_s} \eta(\boldsymbol{\mu})$;
 - 14: Set $M = M + 1$, $\mathcal{P}_{tr} = \mathcal{P}_{tr} \cup \{\boldsymbol{\mu}_{M+1}\}$ and **go to** 1.
 - 15: **end if**
-

In the active data selection algorithm, a natural and simple consideration is to use *standard deviations* to define the error indicator $\eta(\cdot)$ for evaluating the regression model $\hat{\boldsymbol{\pi}}_{\text{GP}}(\cdot)$. Here, one choice of $\eta(\cdot)$ is

$$\eta(\boldsymbol{\mu}) = \sqrt{\sum_{k=1}^{N_h} \sum_{l=1}^L V_{kl}^2 \text{sd}[(\hat{\boldsymbol{\pi}}_{\text{GP}}(\boldsymbol{\mu}))_l]^2},$$

278 analogous to the error in \mathbb{R}^{N_h} -norm, and $\text{sd}[\cdot]$ denotes the standard deviation of a random variable. Each
 279 new active training sample is selected from the pool as the maximizer of the standard-deviation-based error

280 indicator η , and the selection procedure is terminated once a satisfactory prediction quality is achieved.
 281 Alternatively, a desired training sample number M can be defined in advance.

282 Since structural responses with respect to typical structural parameters are usually continuous, even
 283 smooth in most cases, the GPR is accurate even though it is not as powerful as some more advanced
 284 methods in regression, such as *artificial neural networks* (ANNs) [19]. The GPR can provide a natural
 285 and simple standard-deviation-based error indicator in active data selection, and the conciseness of the
 286 GPR model guarantees an efficient procedure of data selection and regression during the offline stage. In
 287 the context of uncertainty quantification, one can take both the uncertainty in the GPR model and the
 288 uncertainty in parameters into account using the Bayesian theory.

289 5. Numerical examples

290 In this section, numerical results for two examples, one in 1D and one in 3D, will be presented to validate
 291 the effectiveness and accuracy of the proposed approach.

292 The FFlagSHyP MATLAB program is used as high-fidelity solver for the numerical examples. The MAT-
 293 LAB version of FFlagSHyP [6] is a program for the finite element analysis of static nonlinear problems in
 294 solid mechanics. Its numerical scheme is introduced in [7, 8]. The two example problems, large deformation
 295 analysis of a trussed frame and that of a twisting column, can also be found in [7] as computational im-
 296 plementations of the nonlinear finite element method. In these numerical examples, the MATLAB function
 297 `fitrgp` is used to construct the GPR models.

298 5.1. One-dimensional example: a trussed frame

299 The first example is a frame made of a beam and a column. As shown in Figure 2(a), the frame is trussed
 300 by 596 one-dimensional elements and loaded by a concentrated load on the beam. The number of DOFs
 301 of the full-order model is $N_h = 476$. Two types of constitutive relations are considered in this problem:
 302 one-dimensional stretch-based hyperelasticity and hyperelasto-plasticity. We refer to [7] for more details of
 303 these constitutive laws. The quantities in Figure 2(a) are given as: Young's modulus $E = 210$ GPa, unit
 304 force $F_0 = 1$ N and unit displacement $\Delta_0 = 1$ mm. With a uniform Young's modulus E in the whole
 305 structure, equilibrium paths, referred to as load-displacement curves, for the two constitutive relations are
 306 shown in Figure 2(b).

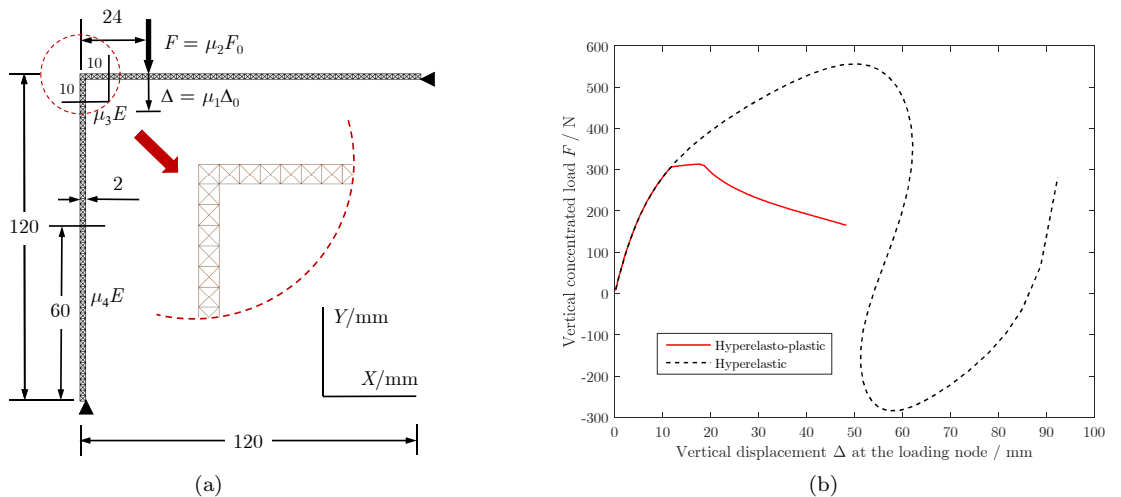


Figure 2: (a) Geometry and input parameters for a trussed frame; (b) Load-displacement curves in both hyperelastic and hyperelasto-plastic cases.

307 This problem is parametrized by four parameters: μ_1 is the quantitative value of the concentrated load
 308 measured in N, μ_2 is the quantitative value of the downward displacement at the loading node, measured

309 in mm, μ_3 is the scaling factor of Young's modulus of a 10 mm \times 10 mm inverted L-shaped zone at the
 310 beam-column joint, and μ_4 is the scaling factor of Young's modulus of the lower half of column. The loading
 311 procedure can be either force-controlled or displacement-controlled, i.e., μ_1 and μ_2 are the two different
 312 controlling parameters of loading, respectively. For the complementary parts of the zones with parametrized
 313 Young's modulus, the modulus is fixed as E . Three parametrized cases will be analyzed as follows.

314 **Case 1:** μ_1 , hyperelasto-plasticity

315 The value of controlling downward deflection Δ for the loading procedure is considered as the only
 316 parameter in this case. The concentrated load is applied to the frame by 40 loading increments with the
 317 arc-length method used, and the size of each increment is determined automatically by the method.

318 After this full-order incremental procedure, 40 high-fidelity solutions with different values of μ_1 are
 319 naturally collected, but those at other values of μ_1 are not available. It is impractical to get the high-fidelity
 320 solution at any parameter value. Thus the 40 full-order solutions are used as snapshots for constructing the
 321 RB space and as training data for the GPR model, i.e. $\Theta = \mathcal{P}_{tr}$. As the 40 training samples are prepared in
 322 advance, active data selection does not make much difference on the computational efforts for training the
 323 GPR model, so the data selection algorithm will not be adopted in this case.

324 The POD for the 40 snapshots gives $L = 5$ bases, and a GPR model with an SE kernel is constructed for
 325 the 5 projection coefficients onto the bases, as shown in Figure 3. In this figure, the prediction curves show
 326 mean values of the GPR outputs, lying in the interval of 95% confidence level. In Figure 3(f), the vertical
 327 displacement Δ at the loading node is extracted from the reduced-order prediction $\hat{\mathbf{u}}_{rb,GPR}(\mu_1) = \mathbf{V}\hat{\boldsymbol{\pi}}_{GP}(\mu_1)$
 328 for each parameter μ_1 in the training samples, matching well with the 'perfect' identical fitting.

329 The average relative error of the projection for $N_s = 40$ snapshots is 0.0033, calculated as

$$\bar{\epsilon}_{\mathbf{v}}(\Theta) = \frac{1}{N_s} \sum_{i=1}^{N_s} \frac{\|\mathbf{u}_h(\boldsymbol{\mu}^i) - \mathbf{V}\mathbf{V}^T\mathbf{u}_h(\boldsymbol{\mu}^i)\|_{\mathbb{R}^{N_s}}}{\|\mathbf{u}_h(\boldsymbol{\mu}^i)\|_{\mathbb{R}^{N_s}}}, \quad (29)$$

330 while the GPR predictions for the training samples $\Theta = \mathcal{P}_{tr}$ have an average relative error $\bar{\epsilon}_t(\Theta) = 0.0154$
 331 compared with the corresponding full-order solutions.

332 **Case 2:** μ_2 , hyperelasto-plasticity

333 The load F is considered as parameter μ_2 in this case. As shown in Figure 2(b), the equilibrium path for
 334 hyperelasto-plastic constitutive relation is not monotone, meaning that the displacement field is multi-valued
 335 with respect to the external load $F = \mu_2$. Thus the regressions for increasing and decreasing stages in the
 336 equilibrium path are carried out separately in this case. Based on 170 training samples, among which 97
 337 are in the increasing stage and 73 are in the decreasing stage, a regression model is obtained by an ANN,
 338 based on *multi-layer perceptrons* (MLPs) [5]. As is well known, the ANN is a powerful tool for nonlinear
 339 regression, so the regression results by the ANN based on the refined set of training data are considered as a
 340 reference. Using the proposed algorithm of active data selection, 85 samples are picked from the 170-sample
 341 set to derive a GPR model. Predictive results by the GPR model are shown in Figure 4. In this figure,
 342 predictions of the projection coefficients, obtained by both the ANN and the GPR, are plotted versus their
 343 'exact' values directly calculated from the full-order solutions. After extracting the vertical displacement
 344 values from the reduced-order solutions by both regression approaches, the corresponding equilibrium paths
 345 are compared in Figure 4(f). It can be seen that the results by the GPR match well with those obtained by
 346 the ANN, even though they are not exactly coincident at some parameter locations in the predictions for
 347 the 5th coefficient. Confirmed by the fact that GPR achieves the similar accuracy with ANN by using half
 348 of the training samples, it supports that GPR is a good choice for the regression method in this context.

349 **Case 3:** $(\mu_3, \mu_4) \in [0.5, 1.5] \times [0.8, 1.2]$, hyperelasticity

350 The parameters μ_3 and μ_4 reflect local material properties and vary in a closed set $\mathcal{P} = [0.5, 1.5] \times [0.8, 1.2]$.
 351 Under the hyperelastic constitutive relation, the configuration under a fixed load $F = 500$ N in the first
 352 increasing stage of equilibrium path (see Figure 2(b)) is taken into account. A Newton-Raphson algorithm
 353 is employed in loading increments until $F = 500$ N is reached. From a set snapshots at $N_s = 25$ randomly
 354 generated points in \mathcal{P} , an RB space of rank $L = 5$ is constructed. Then the active data selection algorithm

355 is adopted to select M training samples from a pool of 400 randomly generated parameter locations. For
356 $M = 50$, the GPR results for the 1st, 3rd and 5th projection coefficients, i.e. the corresponding entries
357 of $\mathbf{V}^T \mathbf{u}_h$, are plotted in Figure 5. During the selection procedure, as M increases, the first 90 parameter
358 positions are shown in Figure 6(a). In this case, $r = 30$ test samples \mathcal{T} with an average relative projection
359 error $\bar{\epsilon}_{\mathbf{V}}(\mathcal{T}) = 1.41 \times 10^{-4}$ are randomly generated to evaluate the prediction quality of the GPR model.
360 As can be seen in Figure 6(b), the average relative error of GPR test predictions is decaying rapidly as
361 M increases from 10 to 50. When the number of selected training samples increases to 40, the order of
362 magnitude of the average relative error decreases to 10^{-4} , showing the accuracy of GPR model and the
363 efficiency of active data selection.

364 **Case 4:** $(\mu_2, \mu_3, \mu_4) \in [0, 530] \times [0.5, 1.5] \times [0.8, 1.2]$, hyperelasticity

365 Three parameters μ_2 , μ_3 and μ_4 are considered in this case. The same full-order samples are used as
366 both the snapshots and the training samples, for which the 50 parameter locations for (μ_3, μ_4) are randomly
367 generated in $[0.5, 1.5] \times [0.8, 1.2]$, and the 20 locations for μ_2 are determined by the arc-length method for
368 loading increments. Note that $N_s = M = 1000$, and the 20 increments lie in the first increasing stage in the
369 equilibrium path and are under $F = 530$ N. Then a reduced-order model is obtained with $L = 10$ reduced
370 bases. For the 20-step loading series at 5 new positions in (μ_3, μ_4) , the relative errors of the corresponding
371 reduced order solutions are shown in Figure 7, and their average is $\bar{\epsilon}_t = 1.13 \times 10^{-3}$.

372 5.2. Three-dimensional example: a twisting column

373 The second example considers a three-dimensional column under the torsion of a pair of uniformly
374 distributed pressure loads $p = \mu_1 p_0$ that are opposite to each other, as illustrated in Figure 8. The stress-
375 strain behavior follows a relation of compressible neo-Hookean elasticity [7], with a fixed bulk modulus
376 $K = 5E_0/3$ and a parametrized shear modulus $G = \mu_2 E_0$. The units of load and modulus are given as
377 $p_0 = 1$ and $E_0 = 100$. Thus the problem is parametrized by μ_1 and μ_2 . The full-order solution of this system
378 is obtained via finite element analysis, in which 576 hexahedral elements are employed, Newton-Raphson
379 algorithm is used for the iteration and the number of DOFs is $N_h = 2700$. Taking $\mu_2 = 1.0$, twisting
380 configurations of the column at different loading stages are shown in Figure 8.

381 **Case 1:** $\mu_1 \in]0, 130[$

382 The magnitude of pressure load is considered as the only parameter μ_1 in this case. High-fidelity solutions
383 at 50 loading increments are prepared in advance, with μ_1 approaching 130. $N_s = 25$ of them with even
384 sequence numbers are taken as snapshots, from which an RB space of $L = 10$ dimensions is constructed.
385 If projecting all the 50 full-order solutions onto the RB space and using them as training data, a GPR
386 model can be trained with an average relative error 1.70×10^{-3} of GPR predictive approximations for the
387 50 samples. When active data selection is adopted with a predictive error tolerance $\text{tol} = 4 \times 10^{-3}$, as
388 introduced in Algorithm 4, 28 training samples are selected. The GPR model obtained is shown in Figure
389 10(a). In this figure, displacement u_X in the X -direction at node B, labelled in Figure 8, is extracted from
390 the reduced-order solution $\tilde{\mathbf{u}}_{\text{rb,GPR}}(\cdot) = \mathbf{V} \hat{\boldsymbol{\pi}}_{\text{GP}}(\cdot)$, and plotted versus μ_1 . The derivative of this displacement
391 with respect to μ_1 , i.e. $du_X/d\mu_1$, is then calculated from the same GPR model, as discussed in Remark 4,
392 and shown in Figure 10(b).

393 **Case 2:** $(\mu_1, \mu_2) \in]0, 40] \times [0.8, 1.2]$

394 In this case, the parameter pair (μ_1, μ_2) varies in $]0, 40] \times [0.8, 1.2]$. Snapshots are calculated at $N_s = 25$
395 randomly picked parameter points to construct an RB space of rank $L = 6$. From a pool of 10×11 parameter
396 locations, 40 are selected as training samples, based on which a GPR model with the ARD SE kernel is
397 derived with an average relative error of 2.1×10^{-3} for test samples. As in Figure 11, the 40 selected
398 parameter locations are labelled, and the predictive results for u_X at node B are plotted.

399 Furthermore, three computational times are compared in Figure 12; the time for calculating one full-
400 order solution at $(\mu_1, \mu_2) = (20, 1.0)$, average time for 40 loops of GPRs in the active data selection, and
401 average time for the calculation of 861 predictive outputs for test samples. One can see that the regressions
402 are recovered very efficiently, and direct outputs from the GPR model in the online stage are obtained at
403 low cost, providing an efficient tool for solving parametrized nonlinear problems.

404 **Remark 5:** We would like to comment on the comparisons between the conventional RB method based
405 on online Galerkin-projections and the regression-based RB method in this paper. In the regression-based
406 approach, the regression models have to be constructed in the offline stage, which means more offline
407 computational efforts. However, this approach only requires direct outputs to obtain the combination
408 coefficients of the RB functions. Compared with the online assemblies and solutions in the conventional RB
409 framework, the regression-based one ensures much higher online efficiency, which better meets the demands
410 of engineering applications. In the context of structural analysis, the nonlinearities could result into some
411 difficulties in the online solutions for the reduced models in the conventional approach, then the accuracy
412 of these reduced-order solutions may be unsatisfactory. We would like to refer to [21], in which the online
413 accuracy and efficiency are quantitatively compared between these two approaches in a nonlinear example.

414 6. Conclusions

415 A non-intrusive RB method is proposed for the ROM of parametrized nonlinear structural problems. In
416 the framework of this method, an RB space is constructed offline by POD as the low-rank approximation
417 to the space spanned by a collection of full-order snapshots. Rather than the conventionally used Galerkin
418 projection scheme, a regression-based approach is adopted to determine the reduced-order solution for any
419 desired new parameter value. Based on the offline establishment of a GPR model between parameter
420 values and projection coefficients, only direct outputs from the model are required during the online stage
421 to obtain the reduced-order solutions at new parameter locations. Hence, the regression-based approach
422 ensures a full decoupling between offline and online stages, and is non-intrusive. With both the accuracy
423 and the efficiency validated by numerical examples, the proposed RB method is shown to be a powerful tool
424 for solving parametrized nonlinear structural problems.

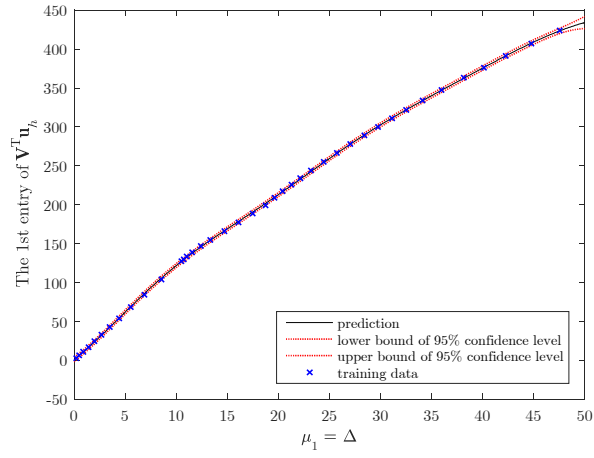
425 In multi-query and real-time contexts of structural analysis, the proposed scheme is able to reduce the
426 model order effectively with a controlled loss of accuracy, and can achieve fast and reliable online calculations
427 for desired parameter values, saving the high computational cost of full-order solutions. This provides a
428 promising technique for the CAE softwares of large-scale structural systems.

429 References

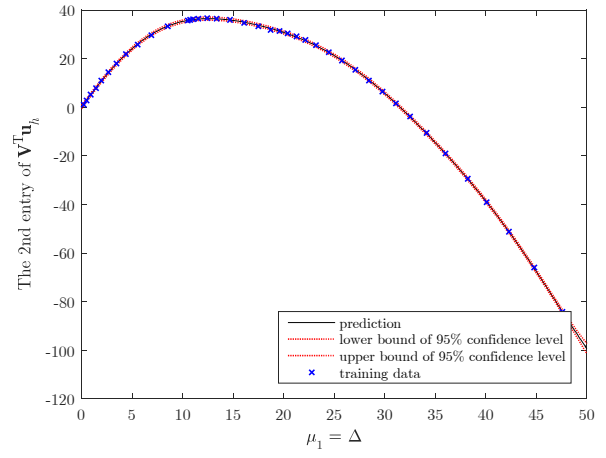
- 430 [1] D. Amsallem, J. Cortial, K. Carlberg, and C. Farhat. A method for interpolating on manifolds structural dynamics
431 reduced-order models. *International journal for numerical methods in engineering*, 80(9):1241–1258, 2009.
- 432 [2] M. Barrault, Y. Maday, N. C. Nguyen, and A. T. Patera. An empirical interpolation method: application to efficient
433 reduced-basis discretization of partial differential equations. *Comptes Rendus Mathematique*, 339(9):667–672, 2004.
- 434 [3] K.-J. Bathe. *Finite Element Procedures*. Klaus-Jurgen Bathe, 2006.
- 435 [4] J. Beck and S. Guillas. Sequential design with mutual information for computer experiments (mice): Emulation of a
436 tsunami model. *SIAM/ASA Journal on Uncertainty Quantification*, 4(1):739–766, 2016.
- 437 [5] C. M. Bishop. *Pattern Recognition and Machine Learning*. Springer, 2006.
- 438 [6] J. Bonet, A. J. Gil, and R. D. Wood. *FLagSHyP software*. <http://www.flagshyp.com>, attached to *Nonlinear Solid
439 Mechanics for Finite Element Analysis: Statics*, Cambridge University Press, 2016.
- 440 [7] J. Bonet, A. J. Gil, and R. D. Wood. *Nonlinear Solid Mechanics for Finite Element Analysis: Statics*. Cambridge
441 University Press, 2016.
- 442 [8] J. Bonet and R. D. Wood. *Nonlinear Continuum Mechanics for Finite Element Analysis*. Cambridge university press,
443 1997.
- 444 [9] D. Bonomi, A. Manzoni, and A. Quarteroni. A matrix discrete empirical interpolation method for the efficient model
445 reduction of parametrized nonlinear pdes: application to nonlinear elasticity problems. MATHICSE Technical Report,
446 EPFL, 2016.
- 447 [10] P. F. Brown, V. J. D. Pietra, S. A. D. Pietra, and R. L. Mercer. The mathematics of statistical machine translation:
448 Parameter estimation. *Computational linguistics*, 19(2):263–311, 1993.
- 449 [11] K. Carlberg, C. Bou-Mosleh, and C. Farhat. Efficient non-linear model reduction via a least-squares petrov–galerkin projec-
450 tion and compressive tensor approximations. *International Journal for Numerical Methods in Engineering*, 86(2):155–181,
451 2011.
- 452 [12] S. Chaturantabut and D. C. Sorensen. Nonlinear model reduction via discrete empirical interpolation. *SIAM Journal on
453 Scientific Computing*, 32(5):2737–2764, 2010.
- 454 [13] W. Chen, J. S. Hesthaven, B. Junqiang, Z. Yang, and Y. Tihao. A greedy non-intrusive reduced order model for fluid
455 dynamics. Technical report, submitted to American Institute of Aeronautics and Astronautics, 2017.

- 456 [14] K. K. Choi and N.-H. Kim. *Structural Sensitivity Analysis and Optimization 1: Linear Systems*. Springer Science &
457 Business Media, 2006.
- 458 [15] P. G. Ciarlet. *Mathematical Elasticity, Vol. I: Three-dimensional Elasticity*. North-Holland Publishing Co., Amsterdam,
459 1988.
- 460 [16] D. A. Cohn, Z. Ghahramani, and M. I. Jordan. Active learning with statistical models. *Journal of artificial intelligence*
461 *research*, 1996.
- 462 [17] C. Eckart and G. Young. The approximation of one matrix by another of lower rank. *Psychometrika*, 1(3):211–218, 1936.
- 463 [18] M. Guo and H. Zhong. Strict upper and lower bounds for quantities of interest in static response sensitivity analysis.
464 *Applied Mathematical Modelling*, 49:17–34, 2017.
- 465 [19] S. Haykin. *Neural Networks: A Comprehensive Foundation*. Prentice Hall, 1999.
- 466 [20] J. S. Hesthaven, G. Rozza, and B. Stamm. *Certified reduced basis methods for parametrized partial differential equations*.
467 Springer, 2016.
- 468 [21] J. S. Hesthaven and S. Ubbiali. Non-intrusive reduced order modeling of nonlinear problems using neural networks.
469 Technical report, to appear in *Journal of Computational Physics*, 2017.
- 470 [22] C. Jäggli, L. Iapichino, and G. Rozza. An improvement on geometrical parameterizations by transfinite maps. *Comptes*
471 *Rendus Mathématique*, 352(3):263–268, 2014.
- 472 [23] A. Kapoor, K. Grauman, R. Urtasun, and T. Darrell. Active learning with gaussian processes for object categorization.
473 In *Computer Vision, 2007. ICCV 2007. IEEE 11th International Conference on*, pages 1–8. IEEE, 2007.
- 474 [24] J. Ko and Y. Ni. Technology developments in structural health monitoring of large-scale bridges. *Engineering structures*,
475 27(12):1715–1725, 2005.
- 476 [25] P. Krysl, S. Lall, and J. Marsden. Dimensional model reduction in non-linear finite element dynamics of solids and
477 structures. *International Journal for numerical methods in engineering*, 51(4):479–504, 2001.
- 478 [26] Y. Liang, H. Lee, S. Lim, W. Lin, K. Lee, and C. Wu. Proper orthogonal decomposition and its applications part i: Theory.
479 *Journal of Sound and vibration*, 252(3):527–544, 2002.
- 480 [27] D. J. MacKay. Information-based objective functions for active data selection. *Neural computation*, 4(4):590–604, 1992.
- 481 [28] A. Manzoni and F. Negri. Automatic reduction of pdes defined on domains with variable shape. MATHICSE Technical
482 Report, EPFL, 2016.
- 483 [29] R. E. Melchers and A. T. Beck. *Structural Reliability Analysis and Prediction*. John Wiley & Sons, 2017.
- 484 [30] R. Milani, A. Quarteroni, and G. Rozza. Reduced basis method for linear elasticity problems with many parameters.
485 *Computer Methods in Applied Mechanics and Engineering*, 197(51-52):4812–4829, 2008.
- 486 [31] K. P. Murphy. *Machine Learning: A Probabilistic Perspective*. MIT press, 2012.
- 487 [32] F. Negri, A. Manzoni, and D. Amsallem. Efficient model reduction of parametrized systems by matrix discrete empirical
488 interpolation. *Journal of Computational Physics*, 303:431–454, 2015.
- 489 [33] N. Nguyen, H. Men, R. M. Freund, and J. Peraire. Functional regression for state prediction using linear pde models and
490 observations. *SIAM Journal on Scientific Computing*, 38(2):B247–B271, 2016.
- 491 [34] N. C. Nguyen and J. Peraire. Gaussian functional regression for linear partial differential equations. *Computer Methods*
492 *in Applied Mechanics and Engineering*, 287:69–89, 2015.
- 493 [35] N. C. Nguyen and J. Peraire. Gaussian functional regression for output prediction: Model assimilation and experimental
494 design. *Journal of Computational Physics*, 309:52–68, 2016.
- 495 [36] A. K. Noor and J. M. Peters. Reduced basis technique for nonlinear analysis of structures. *Aiaa journal*, 18(4):455–462,
496 1980.
- 497 [37] A. T. Patera and G. Rozza. *Reduced Basis Approximation and A Posteriori Error Estimation for Parametrized Partial*
498 *Differential Equations*. Copyright MIT 2007, MIT Pappalardo Graduate Monographs in Mechanical Engineering,
499 <http://www.augustine.mit.edu>, 2007.
- 500 [38] A. Quarteroni, A. Manzoni, and F. Negri. *Reduced basis methods for partial differential equations: an introduction*,
501 volume 92. Springer, 2015.
- 502 [39] A. Radermacher and S. Reese. Pod-based model reduction with empirical interpolation applied to nonlinear elasticity.
503 *International Journal for Numerical Methods in Engineering*, 107(6):477–495, 2016.
- 504 [40] C. E. Rasmussen and C. K. Williams. *Gaussian Processes for Machine Learning*. MIT press Cambridge, 2006.
- 505 [41] G. Rozza, D. B. P. Huynh, and A. T. Patera. Reduced basis approximation and a posteriori error estimation for affinely
506 parametrized elliptic coercive partial differential equations. *Archives of Computational Methods in Engineering*, 15(3):1,
507 2007.
- 508 [42] E. Schmidt. Zur theorie der linearen und nichtlinearen integralgleichungen. i. teil: Entwicklung willkürlicher funktionen
509 nach systemen vorgeschriebener. *Mathematische Annalen*, 63:433–476, 1907.
- 510 [43] S. Seo, M. Wallat, T. Graepel, and K. Obermayer. Gaussian process regression: Active data selection and test point
511 rejection. In *Neural Networks, 2000. IJCNN 2000, Proceedings of the IEEE-INNS-ENNS International Joint Conference*
512 *on*, volume 3, pages 241–246. IEEE, 2000.
- 513 [44] B. Settles. Active learning literature survey. Technical report, University of Wisconsin, Madison, 2010.
- 514 [45] J. C. Simo and T. J. Hughes. *Computational Inelasticity*. Springer Science & Business Media, 2006.
- 515 [46] C. K. Williams and C. E. Rasmussen. Gaussian processes for regression. In *Advances in neural information processing*
516 *systems*, pages 514–520, 1996.
- 517 [47] L. Zanon and K. Veroy-Grepl. The reduced basis method applied to a finite deformation problem in elasticity. In *Proceeding*
518 *of 3rd ECCOMAS Young Investigators Conference*, 2015.
- 519 [48] O. C. Zienkiewicz, R. L. Taylor, and D. D. Fox. *The Finite Element Method for Solid and Structural Mechanics, 7th*
520 *edition*. Elsevier, 2014.

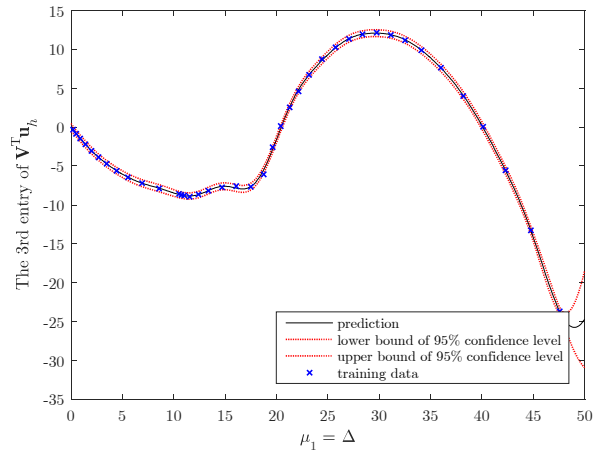
521 [49] O. C. Zienkiewicz, R. L. Taylor, and J. Z. Zhu. *The Finite Element Method: Its Basis and Fundamentals, 7th edition.*
522 Elsevier, 2013.



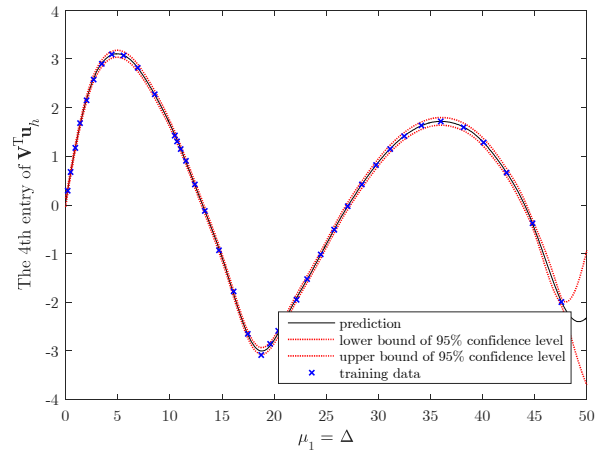
(a)



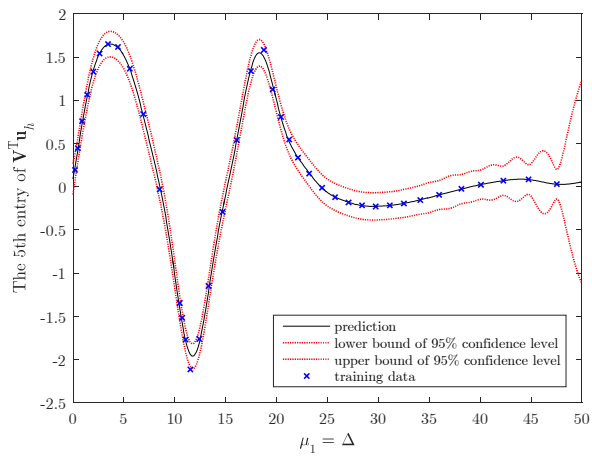
(b)



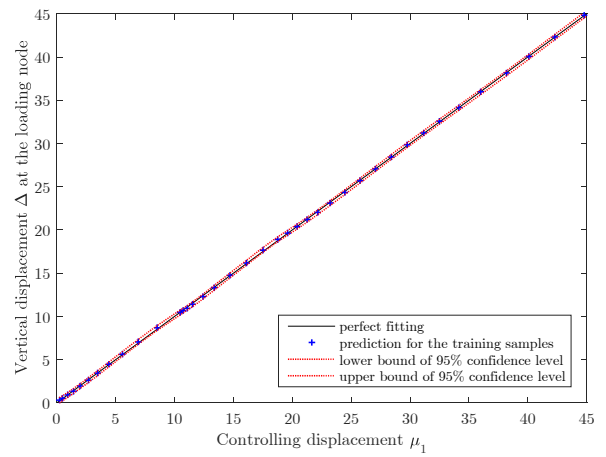
(c)



(d)

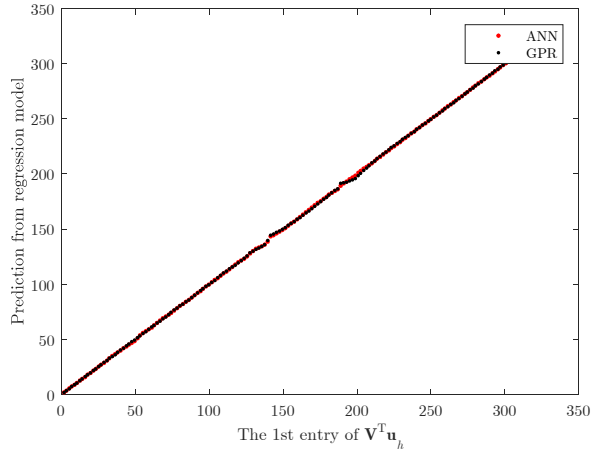


(e)

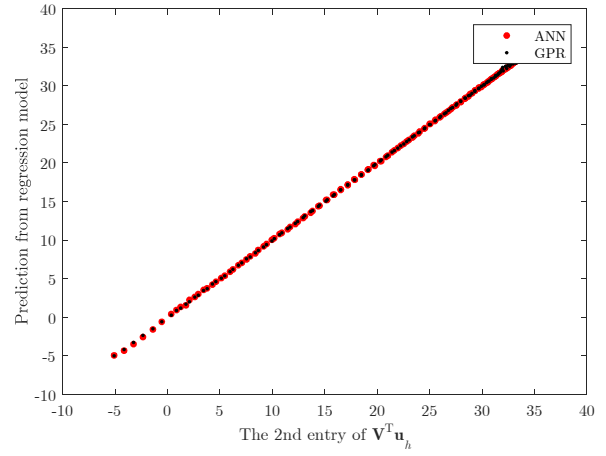


(f)

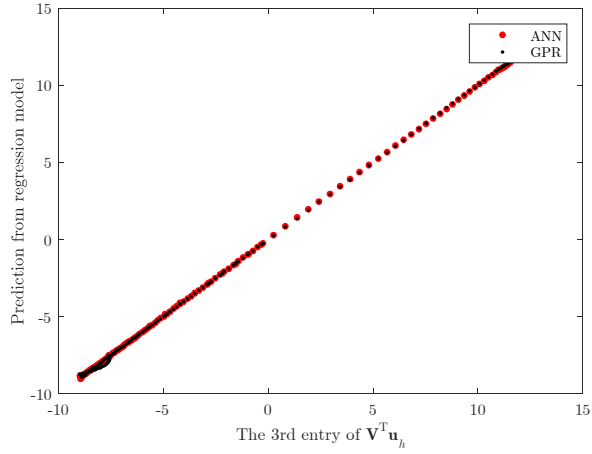
Figure 3: Predictive results by the GPR: (a) – (e) Regression results by the GPR for the 5 entries of $\mathbf{V}^T \mathbf{u}_h$; (f) Extracting vertical displacement Δ at the loading node from the GPR results.



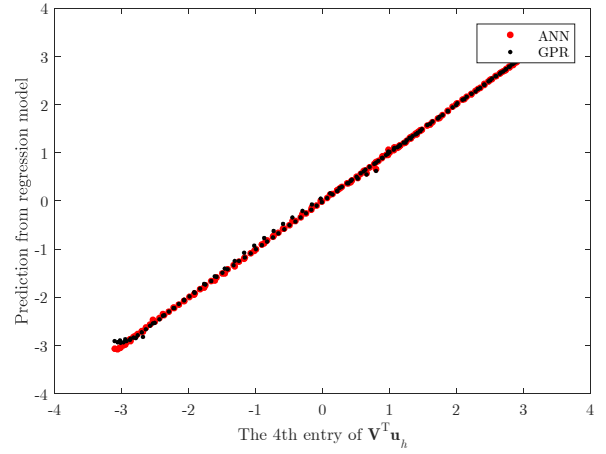
(a)



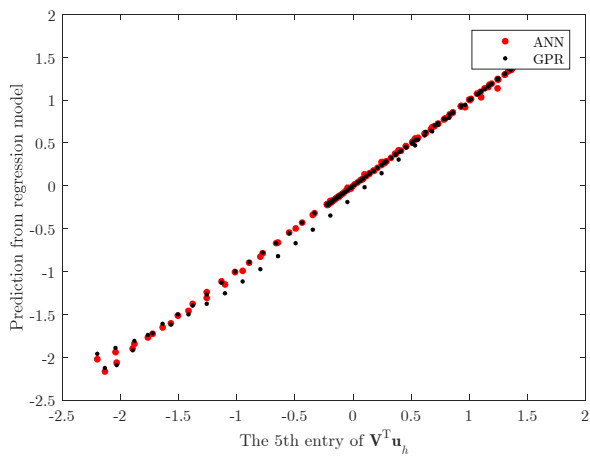
(b)



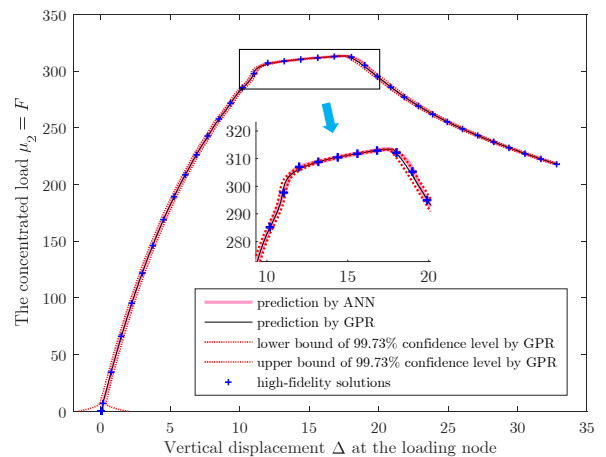
(c)



(d)



(e)



(f)

Figure 4: Predictive results by the GPR and the ANN: (a) – (e) Comparisons of predictive results by the GPR and the ANN for the 5 entries of $\mathbf{V}^T \mathbf{u}_h$; (f) Regression results for the load-displacement curve by both the GPR and the ANN.

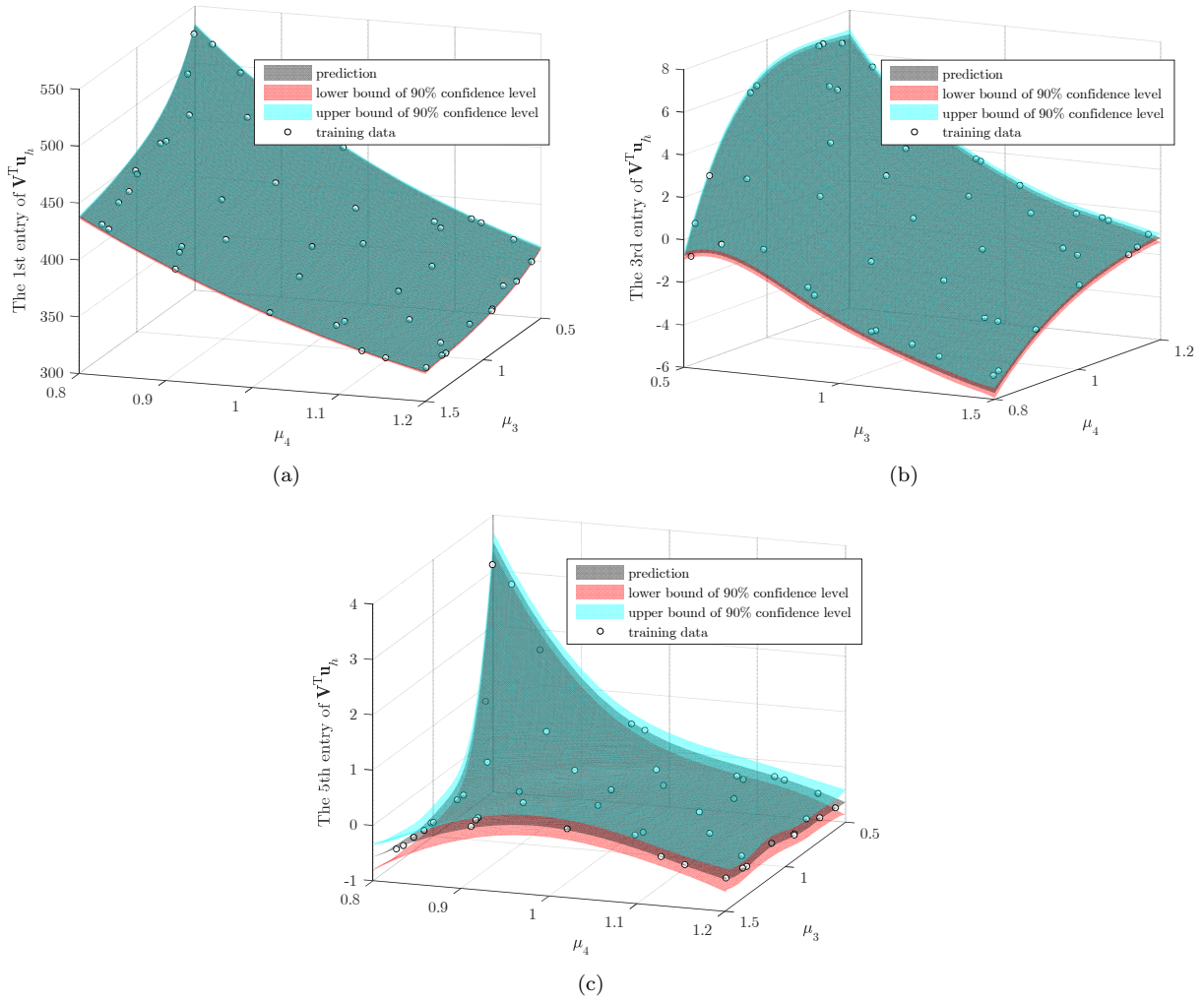


Figure 5: Regression results for the 1st, 3rd and 5th entries of $\mathbf{V}^T \mathbf{u}_h$ from a GPR model trained by 50 samples selected from a pool of 400 parameter values.

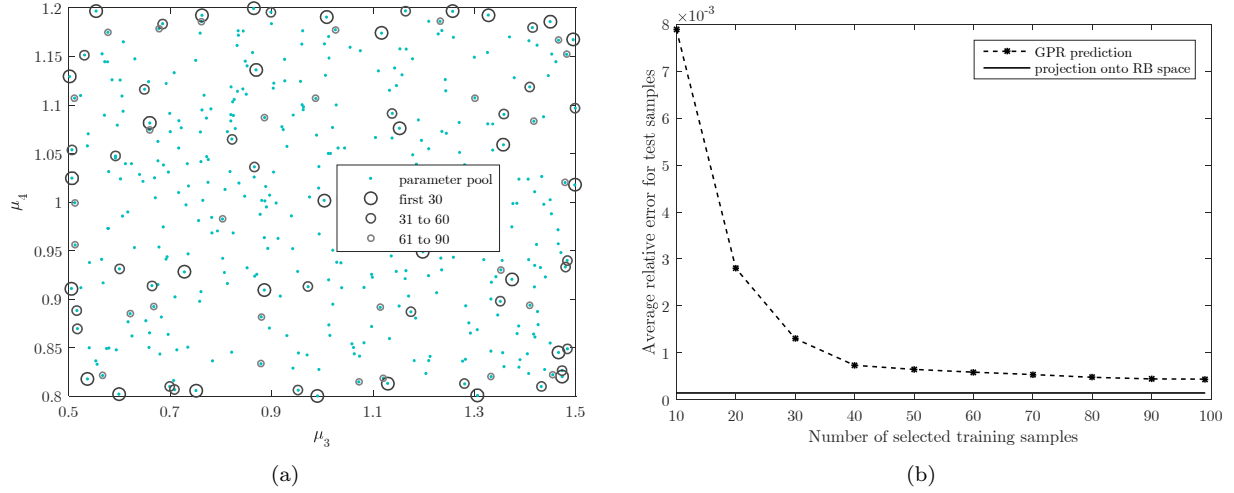


Figure 6: (a) Parameters corresponding to the first 90 samples selected from the pool; (b) Average error decay for 30 testing samples.

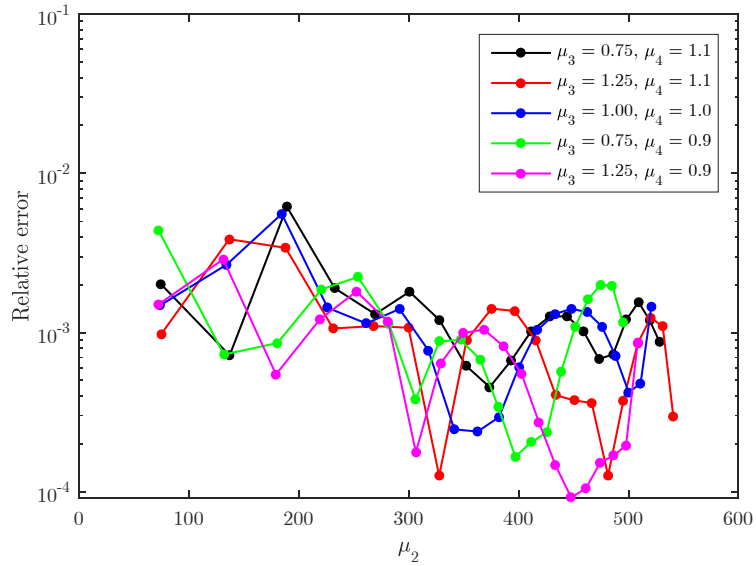


Figure 7: Relative errors of the reduced-order solutions for some test samples compared with the corresponding full-order solutions ($\bar{\epsilon}_t = 1.13 \times 10^{-3}$)

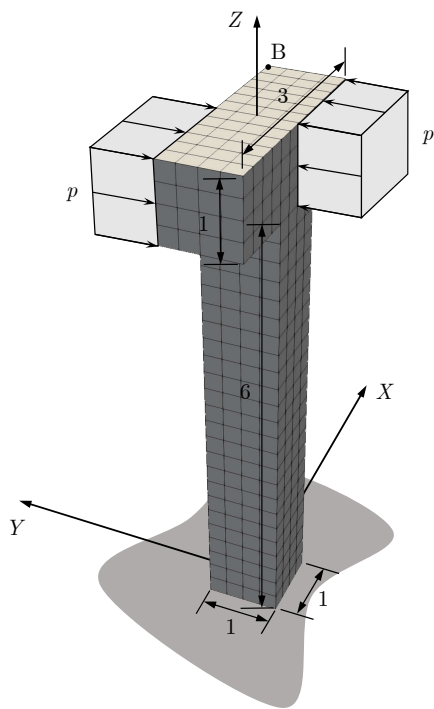


Figure 8: Geometry and pressure loads for the twisting column

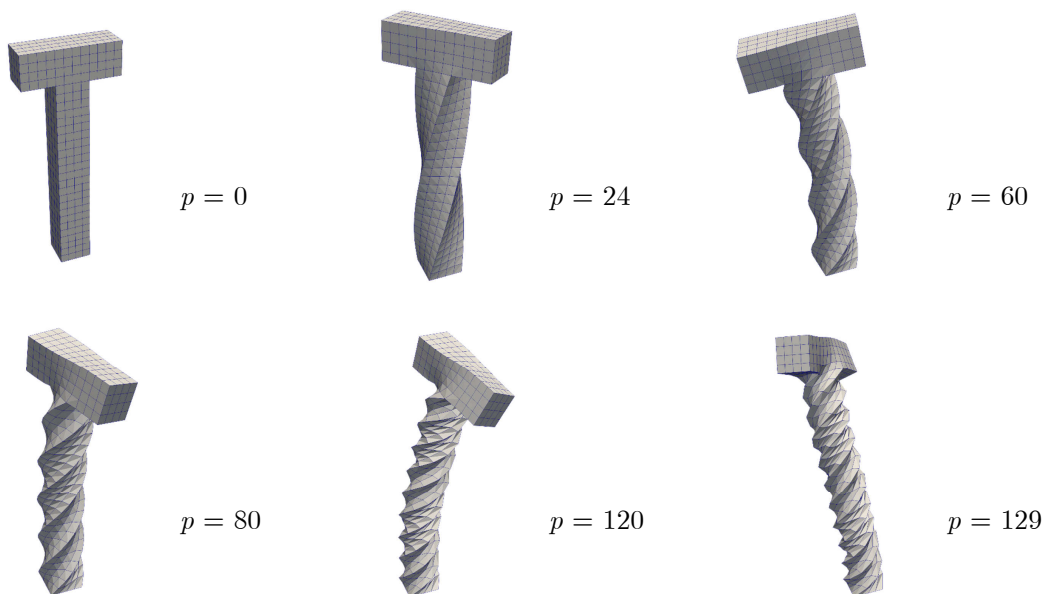


Figure 9: Configurations of the twisting column at different loading stages

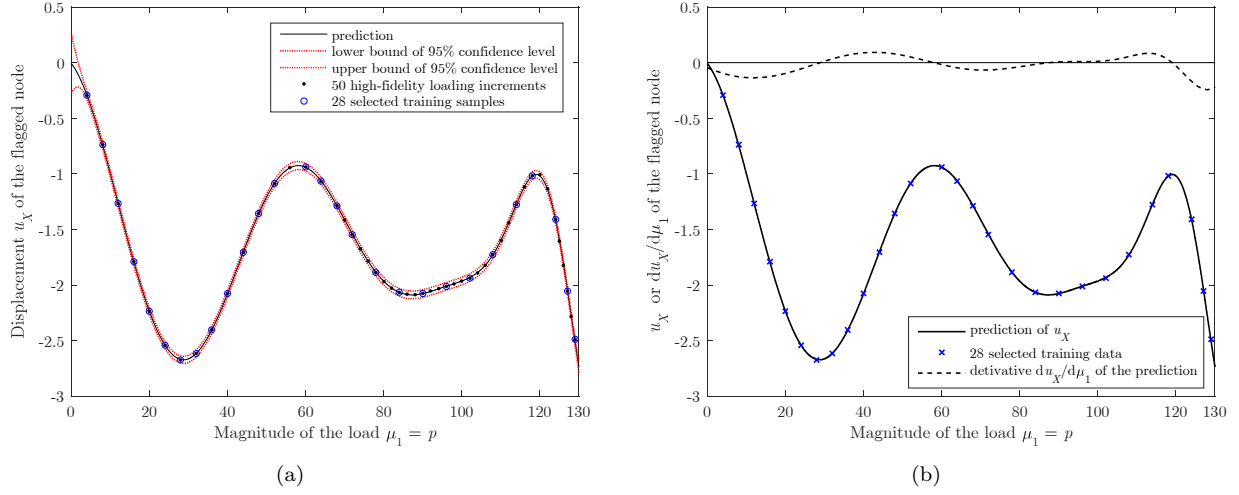


Figure 10: (a) Regression results for the curve of displacement u_X of the labelled node B versus pressure load $\mu_1 = p$; (b) Prediction of u_X at node B and its derivative with respect to μ_1 , both calculated from the GPR model trained by 28 selected samples.

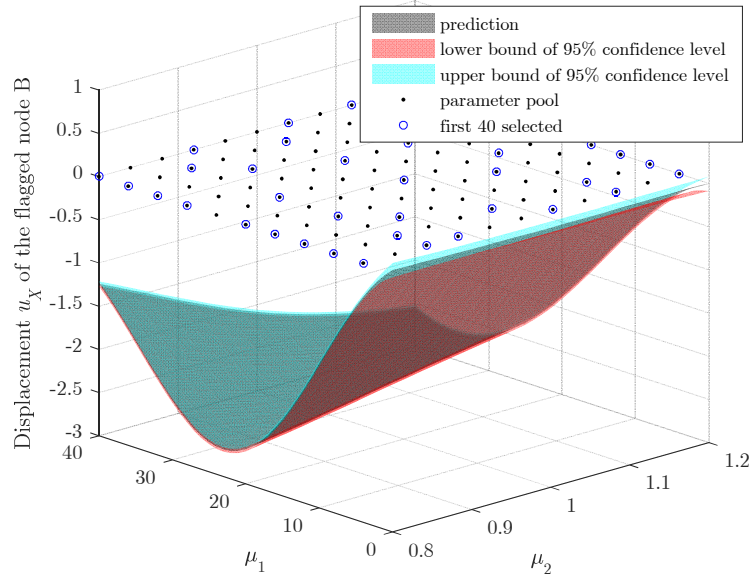


Figure 11: Regression results for the surface of displacement u_X of the labelled node B versus μ_1 and μ_2

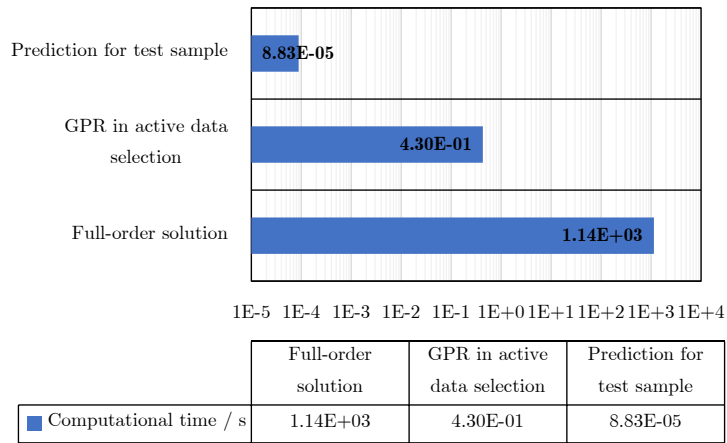


Figure 12: Comparison of times: computational time of a full-order solution at $(\mu_1, \mu_2) = (20, 1.0)$, average time for 40 loops of GPRs in active date selection, and average time for 861 GPR predictive outputs for test samples